Urban Aerosol Impacts on Downwind Convective Storms

SUSAN C. VAN DEN HEEVER AND WILLIAM R. COTTON

Department of Atmospheric Science, Colorado State University, Fort Collins, Colorado

(Manuscript received 13 March 2006, in final form 27 September 2006)

ABSTRACT

The impacts of urban-enhanced aerosol concentrations on convective storm development and precipitation over and downwind of St. Louis, Missouri, are investigated. This is achieved through the use of a cloud-resolving mesoscale model, in which sophisticated land use processes and aerosol microphysics are both incorporated. The results indicate that urban-forced convergence downwind of the city, rather than the presence of greater aerosol concentrations, determines whether storms actually develop in the downwind region. Once convection is initiated, urban-enhanced aerosols can exert a significant effect on the dynamics, microphysics, and precipitation produced by these storms. The model results indicate, however, that the response to urban-enhanced aerosol depends on the background concentrations of aerosols; a weaker response occurs with increasing background aerosol concentrations. The effects of aerosols influence the rate and amount of liquid water and ice produced within these storms, the accumulated surface precipitation, the strength and timing of the updrafts and downdrafts, the longevity of the updrafts, and the strength and influence of the cold pool. Complex, nonlinear relationships and feedbacks between the microphysics and storm dynamics exist, making it difficult to make definitive statements about the effects of urban-enhanced aerosols on downwind precipitation and convection. Because the impacts of urban aerosol on downwind storms decrease with increasing background aerosol concentrations, generalization of these results depends on the unique character of background aerosol for each urban area. For urban centers in coastal areas where background aerosol concentrations may be very low, it is speculated that urban aerosol can have very large influences on convective storm dynamics, microphysics, and precipitation.

1. Introduction

Observations from field campaigns like the Metropolitan Meteorological Experiment (METROMEX) (Braham 1976; Changnon et al. 1981) conducted over St. Louis, Missouri, suggest that large urban regions can influence precipitation and convection occurring over and downwind of such regions. Results from METROMEX indicated that summer precipitation was typically enhanced by 5%–25% over background values within 50–75 km downwind of the urban region (Huff and Vogel 1978; Changnon 1979; Braham et al. 1981, Changnon et al. 1981, 1991). More recent observations in several cities show an increasing thunderstorm frequency associated with increased population growth within these cities (Balling and Brazel 1987; Jaurequi and Romales 1996). Urban regions have also been observed to enhance lightning activity (Westcott 1995; Orville et al. 2001; Steiger et al. 2002; Steiger and Orville 2003). Given the rapidly increasing population of the earth and the enhanced growth rate of urban regions, it is important that we understand how such regions may influence convection and precipitation over and downwind of these regions.

Numerous hypotheses have been proposed to explain the effect of urban regions on convection and precipitation. These include one or a combination of the following: 1) greater aerosol concentrations within urban regions act as cloud condensation nuclei (CCN), giant CCN (GCCN), and ice nuclei (IN) (e.g., Gunn and Phillips 1957; Squires 1958; Squires and Twomey 1961; Warner and Twomey 1967; Warner 1968; Rosenfeld 1999, 2000; Borys et al. 2000, 2003; Ramanathan et al. 2001; Diem and Brown 2003; Andreae et al. 2004; Givati and Rosenfeld 2004; Molders and Olson 2004; Jirak and Cotton 2006); 2) increased surface roughness of urban areas leads to enhanced surface convergence over and downwind of the urban region (e.g., Hjelmfelt 1982; Bornstein and Lin 2000; Craig and Bornstein

Corresponding author address: Susan C. van den Heever, Department of Atmospheric Science, Colorado State University, Fort Collins, CO 80523-1371.
E-mail: sue@atmos.colostate.edu

DOI: 10.1175/JAM2492.1

© 2007 American Meteorological Society

2002; Rozoff et al. 2003); 3) the urban canopy diverts thunderstorms around urban regions (e.g., Loose and Bornstein 1977; Bornstein and Lin 2000); 4) the urban region serves as an enhanced source of moisture (e.g., Dixon and Mote 2003); and 5) sensible and latent heat fluxes within the urban region and thermal perturbations of boundary layer by the urban heat island (UHI) affect moist and dry convection (e.g., Braham et al. 1981; Changnon et al. 1981; Thielen et al. 2000; Baik and Kim 2001; Shepherd et al. 2002; Shepherd and Burian 2003; Rozoff et al. 2003). These effects are discussed in an excellent recent review article by Shepherd (2005) to which the reader is referred for further details. Which of these effects, if any, has the dominant influence has yet to be determined.

The focus of the research presented here is on the impacts of urban-enhanced aerosols on precipitation and convective storms. It has been observed that air pollution produced by industrial and urban regions can act to reduce precipitation in different cloud systems in different regions of the world (Ramanathan et al. 2001; Rosenfeld 1999, 2000; Borys et al. 2000, 2003; Givati and Rosenfeld, 2004; Jirak and Cotton 2006). Air pollutants emanating from an urban area are generally rich in CCN. Enhanced CCN concentrations can suppress warm-rain processes by producing a narrower droplet spectrum that inhibits collision and coalescence processes (e.g., Warner and Twomey 1967; Warner 1968; Rosenfeld 1999). On the other hand, some urban areas, like St. Louis, can also be sources of GCCN, or ultragiant particles, that can enhance warm-rain processes (Johnson 1976; Hindman et al. 1977a,b; Mather 1991; Cooper et al. 1997; Reisin et al. 1996; Feingold et al. 1999; Yin et al. 2000) and thus increase surface precipitation around urban regions.

Enhanced aerosol concentrations also appear to have a significant influence on the storm dynamics and subsequent convective development, as has been observed over Amazonia (Andreae et al. 2004), in simulations of the impacts of maritime and continental aerosol concentrations on deep convection (Khain et al. 2005), and in simulations of tropical convection over Florida (van den Heever et al. 2006). The suppression of the warm-rain process results in a delay in the downdraft development and in greater numbers of cloud droplets and small rain droplets being present within the cloud for longer time periods. These droplets can then be transported to higher altitudes where ice formation is enhanced either through freezing or through interaction with other ice species already present. The presence of supercooled cloud water greatly enhances the rate at which cumuli glaciate by virtue of the fact that supercooled droplets readily collect ice crystals and freeze (Cotton 1972a,b; Koenig and Murray 1976; Scott and Hobbs 1977), as well as by enhancing the Hallett–Mossop rime-splintering process (Cotton and Pielke 1995). The delayed downdraft formation and the latent heat released through ice formation serve to strengthen the updraft, which in turn enhances deep convection. This increases the potential for lightning and heavy precipitation. Therefore, although urban-enhanced aerosol may suppress precipitation initially, it may eventually enhance downwind accumulated precipitation.

Steiger et al. (2002) found, for the 1989–2000 period, that the cloud-to-ground (CG) lightning over Houston, Texas, was enhanced by 45% relative to background rural values and that the largest enhancements occurred in the late morning and afternoon during summer and autumn. They also noted that the enhancement could largely be attributed to the urban influence on large lightning events (>100 flashes) rather than to the increased initiation of new thunderstorms. Stallins et al. (2006) analyzed CG lightning flashes around Atlanta, Georgia, for the 1992–2003 period and found that average annual flash densities over Atlanta were 50%–75% higher than in surrounding rural areas. The urban flash production was found to peak during summer and was more active during the night and early morning hours (1800–0600 local time). Air over Houston is polluted because of the existence of oil refineries and high automobile use and tends to be worst in summer, which corresponds to the time period when the lightning enhancements are the greatest. The reduction in warm-rain processes should lead to enhanced upward transport of supercooled liquid water. Greater amounts of supercooled liquid water, particularly in the $-10°$ to $-20°$C levels where the noninductive charging process is believed to be most efficient, could therefore result in the observed lightning enhancement during the warm season. As shown by Takahashi (1978), higher supercooled liquid water contents should enhance negative noninductive charging of graupel particles at colder temperatures. However, as noted previously, the warm-rain process is also regulated by concentrations of GCCN or ultragiant particles. Thus, it is important to consider not only the concentrations of CCN emitted in urban areas, but also those of GCCN. It is also desirable to consider the urban influences on IN concentrations. Much less is known about urban anomalies in IN, but Braham and Spyers-Duran (1974) suggest that IN are poisoned by the attachment or condensation of sulfates and other hygroscopic materials in urban pollution.

It appears from observations that the impact that urban areas may have on convection, precipitation, and lightning is great, but the nature of the dominant urban

forcing is still not understood well, and the relative importance of the various urban influences discussed above is not well established and may well be unique for a given urban region. The hypotheses presented above require significant testing. Numerical models are useful tools with which to study the effects of urban land use and aerosol/pollution separately and together and hence to establish the relative importance of each of these factors (and perhaps others) on precipitation, convection, and lightning over and downwind of urban areas. However, relatively few numerical modeling studies have been cited in the literature of these urban effects. Shepherd (2005) attributes this to numerous factors, including the poor representation of the urban land surface in models, the oversimplification or inadequate representation of microphysical processes in numerical models, the lack of ability to represent aerosol fields in models, and computing limitations on the inclusion of explicit microphysics, dynamics, aerosol, and land surface characteristics and processes that are needed to simulate a fully coupled atmosphere–land system. For the research presented here, the sophisticated Town Energy Budget (TEB) generalized urban canyon model (Masson 2000; Masson et al. 2002) has been given an interface with the aerosol version (Saleeby and Cotton 2004) of the Regional Atmospheric Modeling System (RAMS) developed at Colorado State University (CSU) (Pielke et al. 1992; Cotton et al. 2003). This allows for the simulation of both the effects of the urban land surface and urban-enhanced aerosols on convection and precipitation downwind of urban environments. Rozoff et al. (2003) have already investigated the impacts of the urban land surface on the convection that developed over and downwind of St. Louis on 8 June 1999. The impacts of urban-enhanced aerosols on convection for the same case study as that used by Rozoff et al. (2003) are investigated in this paper.

The case study chosen to investigate the influences of urban regions on downstream precipitation and convective storms is outlined in the next section. The model used and the experiment setup are described in section 3. The results from simulations with higher and lower background aerosol concentrations are presented in sections 4 and 5, respectively. A discussion of the implications of these results is given in section 6.

2. Case study

Simulations have been conducted of the convective storm development that occurred over and downwind of St. Louis on 8 June 1999. Using the same case study as that of Rozoff et al. (2003) allows for a direct comparison of the land surface effects and the aerosol impacts on these convective storms. On this day ordinary convective thunderstorms occurred around St. Louis. The environment was devoid of large-scale forcing but was warm and moist ($\sim$1500 J kg^{-1} of CAPE). Storms were initiated in the early afternoon and lasted through the early evening (Fig. 1), producing locally heavy rain, large hail, and considerable wind damage in the city of St. Louis, as outlined in the Storm Prediction Center storm-report data.

In METROMEX "airmass" storms were found to occur 116% more frequently downwind of St. Louis than in rural areas (Changnon et al. 1981). Huff and Vogel (1978) found that 43% of the storms affecting the St. Louis area came from the southwest and west-southwest during METROMEX. The relatively weak, southwesterly mean tropospheric flow on 8 June 1999, together with the relatively warm, moist surface and the isolated and transient nature of the storms, provides a case study that is representative of the climatic conditions of METROMEX, is suitable for the study of urban-enhanced storms, and allows for a comparison with the output from Rozoff et al. (2003). Further details of the synoptic environment on this day are included in Rozoff et al. (2003).

3. Model and experiment setup

a. Model configuration

RAMS (Pielke et al. 1992; Cotton et al. 2003), which was used in this study, is a nonhydrostatic cloud-resolving model that utilizes sophisticated microphysics, radiation, surface, and turbulence schemes. Three two-way interactive nested model grids with horizontal grid spacings of 37.5, 7.5, and 1.5 km were centered over St. Louis (Fig. 2). Grids 1 and 2 are used to simulate the synoptic and mesoscale environments, respectively. The grid spacing on the third grid is sufficient to resolve deep convection. Forty vertical levels with variable grid spacing were used, and the model top extended to approximately 22 km above ground level (AGL). Eight of the vertical levels fall within the first 1 km AGL. The long time step was 60 s. RAMS was heterogeneously initialized with data from the Eta Model Data Assimilation System (EDAS; Rogers et al. 1996) from 8 June 1999. These data were also used as time-dependent fields to which the lateral boundary regions of grid 1 are nudged during integration. The basic radiative condition (Klemp and Wilhelmson 1978) was applied to the normal velocity components at the lateral boundaries of grid 1.

The surface processes were parameterized using the Land Ecosystem–Atmosphere Feedback model (LEAF-2; Walko et al. 2000). There are 30 different land surface types included within LEAF-2, most of which are

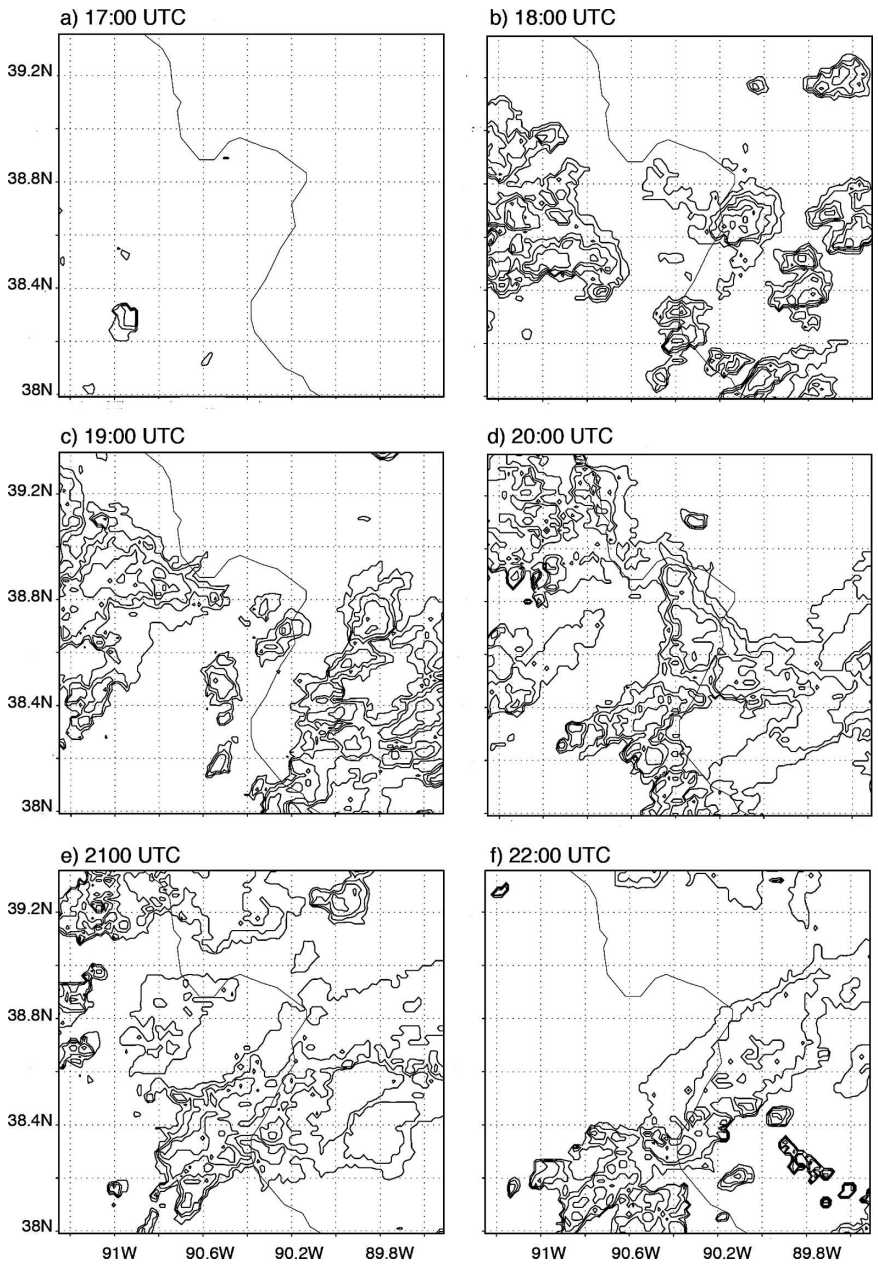

FIG. 1. Composite radar images over St. Louis for (a) 1700, (b) 1800, (c) 1900, (d) 2000, (e) 2100, and (f) 2200 UTC 8 Jun 1999, after Rozoff et al. (2003). The image was adapted with permission of C. Rozoff. Contour intervals are provided every 10 dB*Z*.

defined in the Biosphere–Atmosphere Transfer Scheme (Dickinson et al. 1986). Multiple vegetation patches may be activated within each grid to represent the variation in surface vegetation. For urban regions, the leaf-area index and vegetation fractional coverage are minimized while the roughness length is increased, thereby representing the effects of the rough city surface. Land cover for grids 1 and 2 was obtained from the Advanced Very High Resolution Radiometer–derived Olson Global Ecosystem land cover data from the U.S. Geological Survey Earth Resources Observation System Data Center (Lee 1992), which is at 1-km resolution. The Landsat Thematic Mapper National Land Cover Dataset was used to portray more accurately the heterogeneity of the urban land surface. Further details of the surface initialization are outlined in Rozoff et al. (2003). Soil moisture and temperatures were initialized heterogeneously using EDAS data.

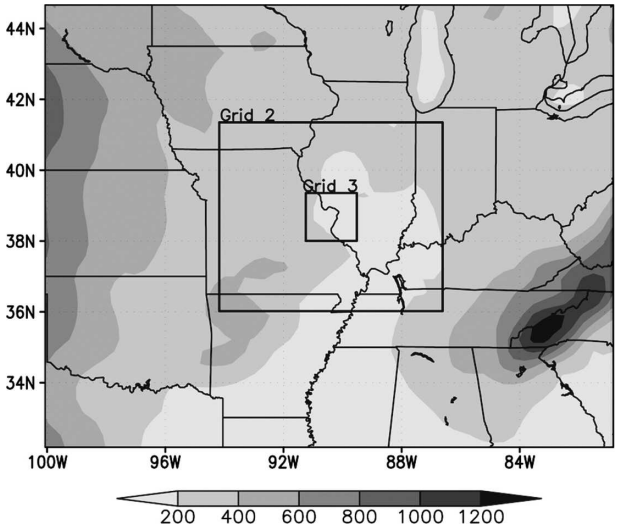

FIG. 2. The location of grids 1–3 for the simulations described in the text. The field shown is topography (m).

The TEB generalized urban canyon model (Masson 2000; Masson et al. 2002) is used in place of the LEAF-2 parameterization for urban regions, thus allowing for a more accurate representation of the three-dimensional urban surface and associated processes. This provides quantities such as sensible heat flux, latent heat flux, momentum covariances, albedo, and emissivity to the first model level. TEB provides these quantities to RAMS as an urban patch contribution at the first model level, from which point they are averaged with the fluxes from LEAF-2 for the nonurban patches for each grid cell. Separate energy budgets are considered for the roofs, walls, and roads. Information is needed to describe building materials, road materials, and the geometry of the urban area. Roofs and walls are made up of three layers, composed of dense concrete, aerated concrete, and insulation, and dry soil overlaid by asphalt constitutes roads. Typical values for these materials are contained in Oke (1988) and Masson (2000) and are summarized in Rozoff et al. (2003). Various other parameters are determined subjectively from recent aerial photographs of St. Louis. An average building height of 15 m, with building and canyon aspect ratios of 1, and a roughness length of 0.8 m were used here and represent the average St. Louis land-class characteristics. Sensible and latent heat fluxes generated by urban traffic and industrial processes are also accounted for. It is possible to vary the different TEB parameters; however, this has not been done for the simulations presented here.

The mixing ratios and number concentrations of the various hydrometeors were predicted through the use of a two-moment bulk microphysical scheme (Meyers et al. 1997). The main difference between bulk and bin microphysical schemes is that in bulk schemes the shapes of the size distribution of the various hydrometeors are prescribed a priori, whereas in the bin approach these are calculated during the model integration and thus can vary with time. The use of bulk microphysical approaches also often introduces the need for further assumptions such as the utilization of mean sedimentation velocities. As such, bulk microphysical schemes will have an impact on the microphysical processes dependant on changes in the shape of hydrometeor size distributions and can lead to inaccuracies in hydrometeor locations with height and precipitation amounts. The bin approach generally leads to a more accurate representation of hydrometeor interactions and precipitation processes. However, the intense computational needs of such schemes frequently limit their use to simulations that are two-dimensional or to short-lived idealized three-dimensional experiments, although recently a first attempt at using a simplified "fast" bin microphysical approach on the innermost grid in a nested grid model was successfully made (Lynn et al. 2005a,b).

Although a two-moment bulk scheme is used for this research, it does not follow the method spearheaded by Kessler (1969). Instead, the approach attempts to represent the essence of bin-resolved microphysics models. For example, the activation of CCN is parameterized through the use of a detailed bin-resolving Lagrangian parcel model developed by Feingold and Heymsfield (1992). Assuming that CCN are ammonium sulfate particles having a lognormal size distribution, Saleeby and Cotton (2004) developed a lookup table that considers ambient cloud conditions for the nucleation of cloud droplets from aerosol. Likewise, in the two-moment scheme the cloud droplet spectrum is decomposed into two modes—one for droplets 1–40 μm in diameter and the second for droplets 40–80 μm in diameter. This bimodal cloud droplet size distribution allows for a more accurate representation of droplet collection of the bimodal droplet distribution that often occurs in the atmosphere. The cloud droplets are nucleated based on the activation of CCN and GCCN. Cloud droplet concentrations are therefore predicted based on the CCN and GCCN concentrations and collection processes. Collection is simulated using stochastic collection equation solutions (Feingold et al. 1988), facilitated by lookup tables, rather than by continuous accretion approximations. The philosophy of bin representation of collection is extended to calculations of drop sedimentation (Feingold et al. 1998). The accuracy of this approach has had some limited evaluation against two-moment bin-resolving representations of marine stra-

TABLE 1. RAMS model configurations and options.

Model aspect	Setting
Grid	Arakawa C grid (Mesinger and Arakawa 1976)
	Horizontal grid
	Grid 1: $\Delta x = \Delta y = 37.5$ km; 50×40 points
	Grid 2: $\Delta x = \Delta y = 7.5$ km; 92×82 points
	Grid 3: $\Delta x = \Delta y = 1.5$ km; 102×102 points
	Vertical grid: 40 vertical levels; Δz variable
	Model top: ~22 km
	Eight levels below 1 km AGL
Initialization	40-km Eta data
	Aerosol concentrations obtained from METROMEX
Time step	60 s
Simulation duration	26 h
Microphysics scheme	Two-moment bulk microphysics (Meyers et al. 1997)
	Vapor, cloud water, rain, pristine ice, snow, aggregates, graupel, and hail all activated
Convective initiation	No cumulus parameterization; convection is explicitly simulated
Boundary conditions	Radiative lateral boundary (Klemp and Wilhelmson 1978)
Turbulence scheme	Smagorinsky (1963) deformation K closure scheme with stability modifications by Lilly (1962) and Hill (1974)
Radiation scheme	Harrington (1997)
Surface scheme	LEAF-2 (Walko et al. 2000) coupled with the TEB model (Masson 2000) for urban regions

tocumulus clouds (Feingold et al. 1998), but there has been no systematic evaluation of the accuracy of this approach in the application to deep convective clouds. It is possible that it has similar accuracy to that of a single-moment bin model with a limited number of bins, but that is pure conjecture at this point. The water species that are activated for these simulations include pristine ice, snow, aggregates, graupel, hail, cloud water, and rain. The various model configuration and options used for the simulations presented here are summarized in Table 1.

b. Experiment design

Rural and urban CCN and GCCN concentrations are required to initialize these fields in the model, after which the concentrations of these species are prognosticated. The initial CCN and GCCN concentrations were estimated using observations made during METROMEX. Upwind and downwind summer CCN concentrations made between 1971 and 1973 (Braham 1974; Spyers-Duran 1974; Auer 1975) at 0.7% supersaturation were averaged, resulting in rural and urban CCN concentrations of 1200 and 2000 cm^{-3}, respectively. GCCN (>1 μm in radius) concentrations were obtained from volume distributions of large aerosol particles (diameters between 5 and 55 μm) upwind and downwind of St. Louis (Johnson 1976; Braham 1977) and were combined with concentrations obtained for particle sizes between 1 and 5 μm from volume distributions presented by Komp and Auer (1978). The rural and urban GCCN concentrations were found to be 0.1 and 0.2 cm^{-3}, respectively. METROMEX data were used rather than data from more current sources because CCN and GCCN concentrations can only be inferred from the available current data, whereas during METROMEX, precise measurements of these aerosol species were made.

In the control experiment (RURAL-H), the urban region and the associated urban surface characteristics and heat and moisture fluxes are activated but the entire model domain is initialized with the rural CCN and GCCN concentrations given above. Sensitivity tests were then conducted in which a continuous source function of CCN (CCN-H), GCCN (GCCN-H), and then both CCN and GCCN (URBAN-H) was activated over the urban region. The source function was such that the CCN and/or GCCN concentrations between the surface and approximately 500 m AGL over the urban region were set at each time step to the urban concentrations of each species. The model was initialized with the rural aerosol concentrations elsewhere. These four simulations were then repeated, but the impacts of the urban region were removed by replacing the urban land use class with cropland, and the suburban land class with wooded grassland. The aerosol characteristics were, however, maintained, thus allowing for a comparison of the momentum and energy effects of the urban region with the aerosol effects. The characteristics of these sensitivity tests are summarized in Table 2. Only one of the experiments in which the urban region was removed is indicated in this table for the sake of simplicity.

TABLE 2. Aerosol initialization concentrations for the sensitivity tests described in the text (here R denotes rural and U denotes urban).

Expt	CCN	GCCN	CITY	Notes
High background aerosol concentrations				
RURAL-H	R	R	On	Rural has CCN = 1200 cm^{-3} and GCCN = 0.1 cm^{-3}; urban has CCN = 2000 cm^{-3} and GCCN = 0.2 cm^{-3}
CCN-H	U	R	On	
GCCN-H	R	U	On	
URBAN-H	U	U	On	
NOCITY-H	R	R	Off	
Lower background aerosol concentrations				
RURAL-L	R	R	On	Rural has CCN = 800 cm^{-3} and GCCN = 0.01 cm^{-3}; urban has CCN = 2000 cm^{-3} and GCCN = 0.2 cm^{-3}
CCN-L	U	R	On	
GCCN-L	R	U	On	
URBAN-L	U	U	On	

Although similar concentrations are often observed over the central United States (J. Hudson 2005, personal communication), the rural concentrations are relatively high. To investigate the impacts of urban-enhanced aerosol on downwind convection for situations in which the rural aerosol concentrations are lower, such as was observed during some periods of METROMEX and such as may be found in other regions of the United States as well as in areas of Canada and Australia and other less industrialized nations, the series of experiments just described was then repeated using lower background concentrations of 800 cm^{-3} for the CCN concentrations and 0.01 cm^{-3} for the GCCN concentrations. The urban aerosol concentrations were kept the same as those used in the first series of experiments. The details of this series of experiments are also summarized in Table 2. Note that the tests with the higher background aerosol concentrations will be denoted using "-H" and those with lower background aerosol concentrations will be denoted with "-L." The focus will primarily be on the tests with lower background aerosol concentrations because the differences are greater in this set of experiments. However, many of the trends observed are evident in both series of tests.

Numerous calculations have been performed for the region downwind of the urban area. The area used for these calculations is shown in Fig. 3. It is apparent

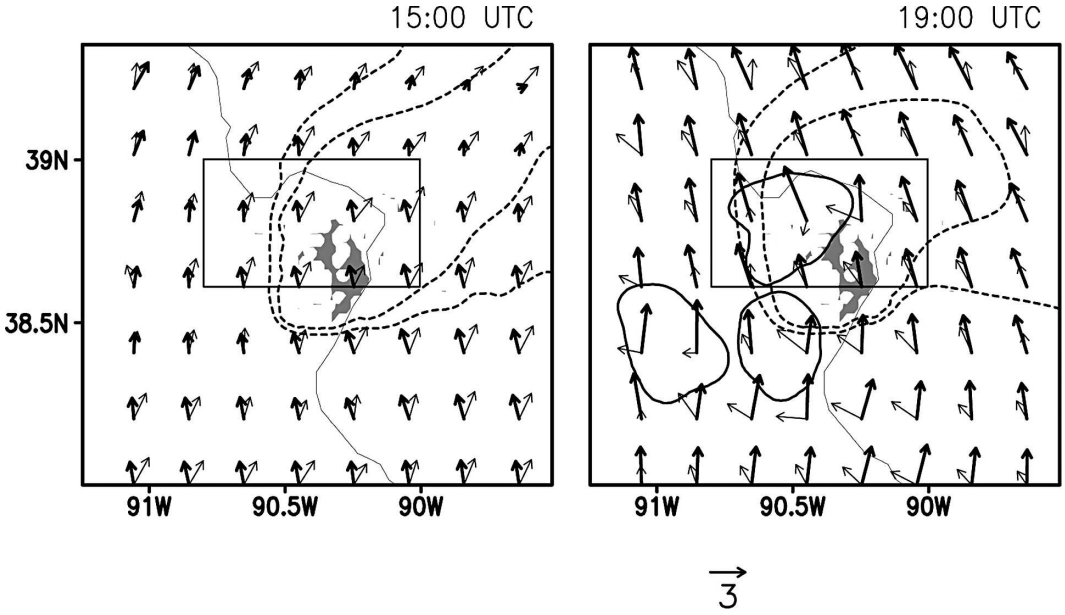

FIG. 3. The location of the downwind calculations referred to in the text is shown by the rectangular box. CCN concentration isolines (1300 and 1500 cm^{-3}) at 270 m AGL are indicated by the dotted lines, and St. Louis is shown by the shading. The wind vectors at the surface and at ~1600 m AGL are indicated by the thin and thick vectors, respectively. These fields are shown at (left) 1500 and (right) 1900 UTC. The 1-mm accumulated precipitation isoline at 2200 UTC is shown in the right panel by the solid dark lines.

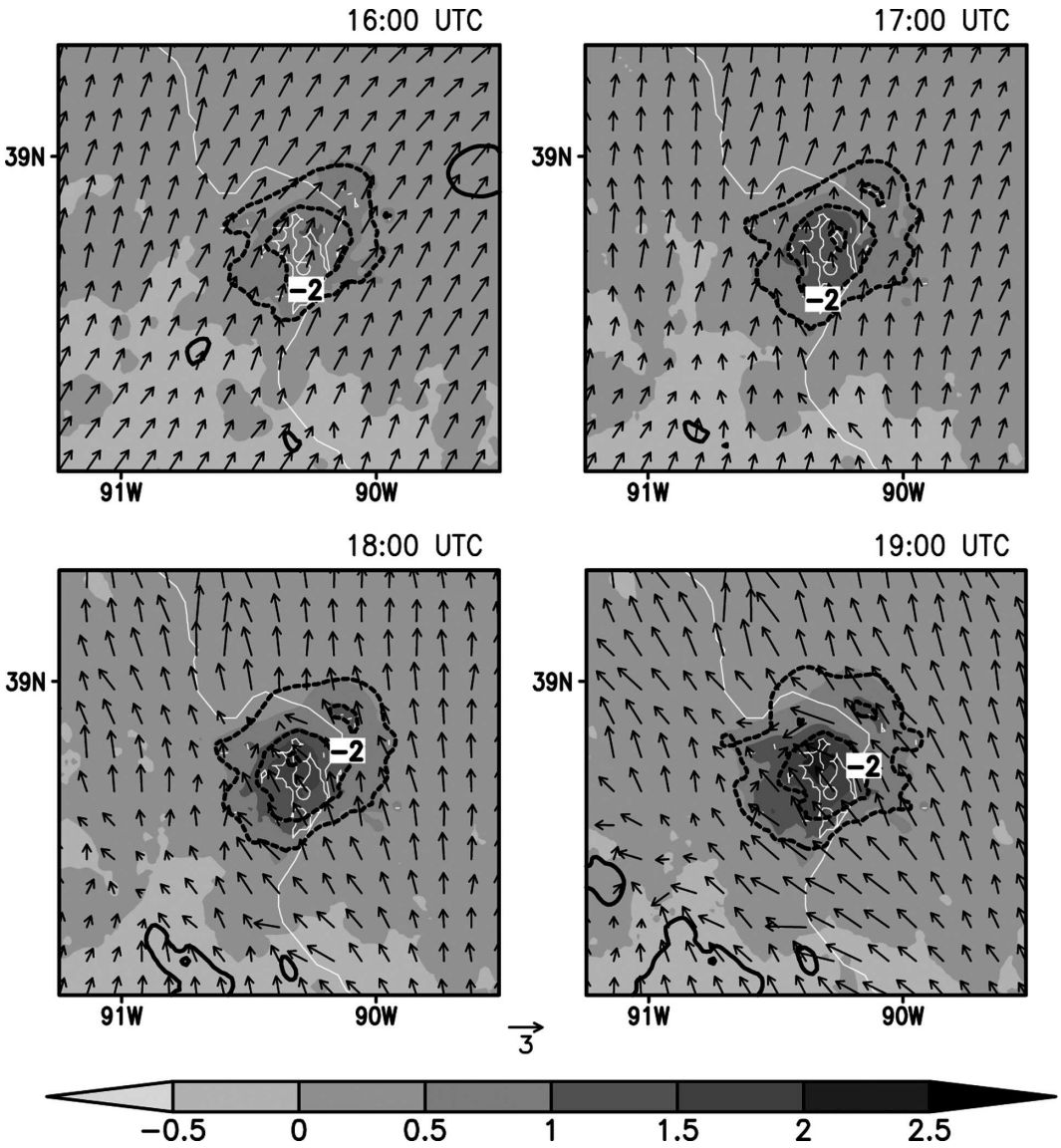

FIG. 4. Time evolution of the RURAL-H − NOCITY-H temperature and water vapor mixing ratio fields at the lowest model level (48 m). Temperature (°C) is shaded, water vapor mixing ratio (g kg^{-1}) is indicated using thick black contours at 1 g kg^{-1} intervals, and rivers and St. Louis are indicated using thin white lines. Wind vectors for the RURAL-H are also indicated, the scale of which is indicated at the bottom of the figure.

from Fig. 3 that the winds at the surface and at 1600 m AGL are from the southwest and southeast before and during the time period of interest (1900–2200 UTC) and that the area downwind of St. Louis is therefore to the northwest, north, and northeast of the city. This area was also chosen because by 2200 UTC the accumulated precipitation produced by the storms developing downwind of the city falls completely within this region (Fig. 3b) and the precipitation produced by the storms that develop upwind of the city of the city is excluded.

4. Higher background aerosol concentration results

All the simulations in which the urban region is included produce a UHI during the daytime of 8 June 1999. In Fig. 4 the evolution of the UHI from 1600 to 1900 UTC, represented as the difference in the temperature fields between the RURAL-H and NOCITY-H simulations, is shown. The UHI begins intensifying around 1600 UTC, and by 1800 UTC a heat island of approximately 2°C has formed. Water vapor

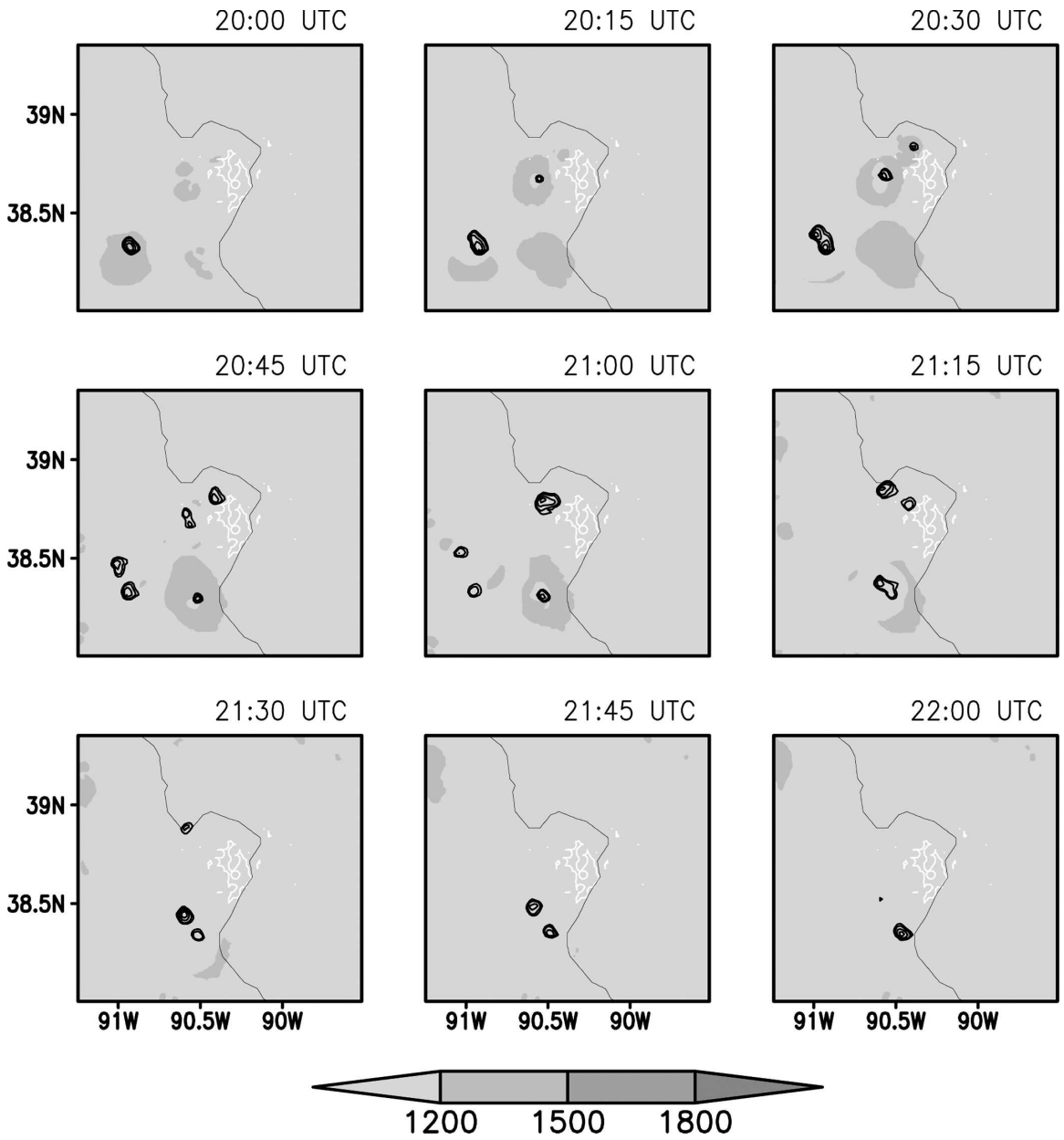

FIG. 5. Storm evolution for RURAL-H simulation. CCN concentrations (cm^{-3}) at ~550 m AGL are shaded and updraft velocity ($m\ s^{-1}$) at ~10 750 m AGL is contoured at 10 $m\ s^{-1}$ using thick black lines. The 5 $m\ s^{-1}$ isoline is also included. St. Louis is indicated using white lines.

mixing ratios over the city are lower than over the surrounding rural regions. Convergence of the wind flow both over and downwind of the urban region, similar to that observed previously in the literature (e.g., Hjelmfelt 1982; Bornstein and Lin 2000; Craig and Bornstein 2002; Rozoff et al. 2003; Shepherd 2005), strengthens throughout the morning. The winds are southwesterly initially and back as the morning progresses, becoming more southeasterly by 1900 UTC. In the observations the winds tend to be more southwesterly. Similar results were found by Rozoff et al. (2003).

Examining the storm development for the RURAL-H case (Fig. 5), it is apparent that convection occurs both downwind (or to the northwest) of St. Louis, as well as to the southwest of the city. Convection develops around 1945 UTC and lasts to around 0000 UTC (not shown). The storm location around the city is similar to the storms observed on this day (Fig. 1), although the

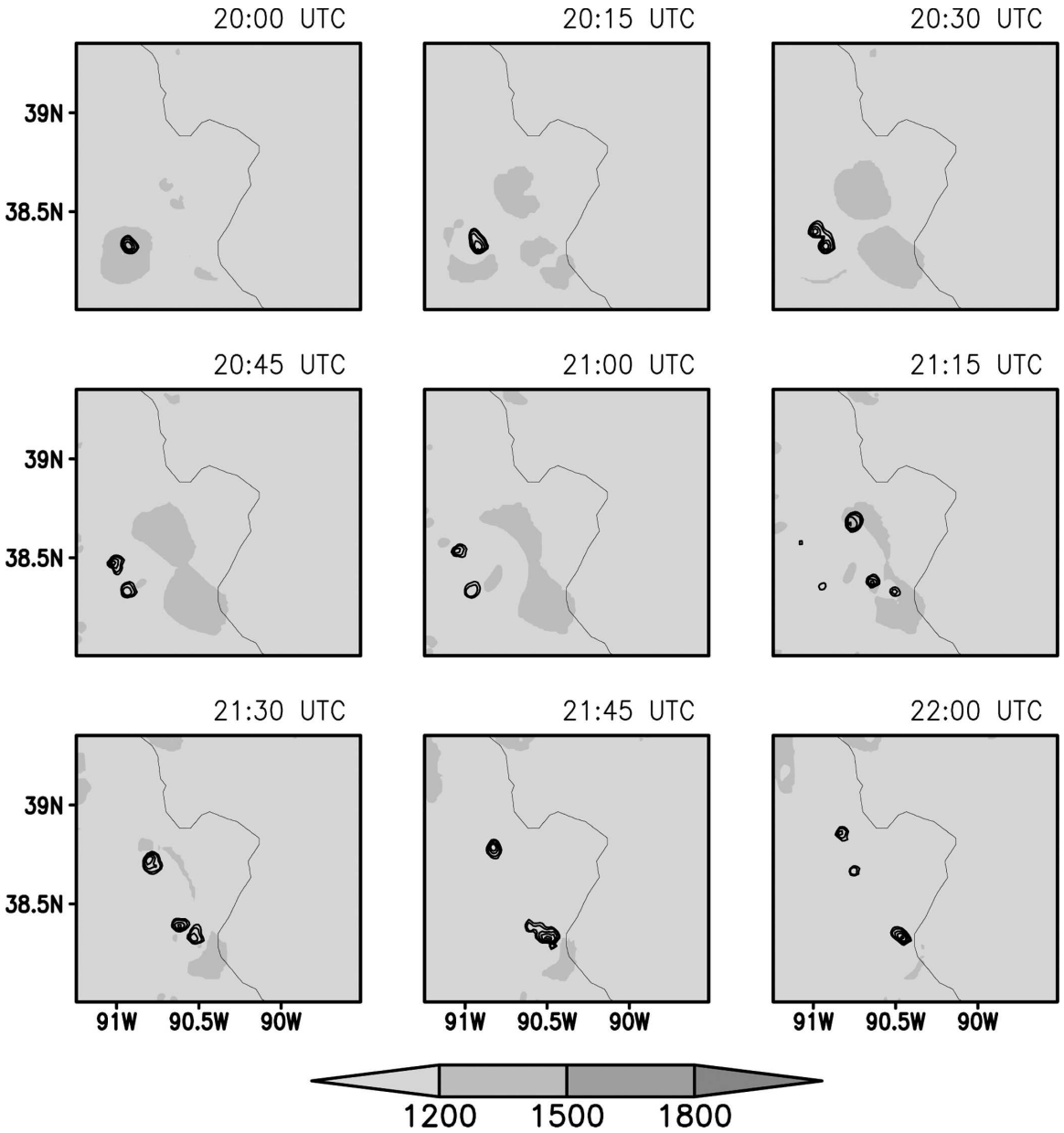

FIG. 6. Same as in Fig. 5, but for NOCITY-H. St. Louis is not indicated because the urban region is not included in this sensitivity test.

development of the simulated storms lags that of the observed storms by about 2 h, as observed by Rozoff et al. (2003). Note that the storms observed to the east of the city are not well represented in these simulations because they are located right along the eastern boundary of grid 3.

In comparing the storm development in the RURAL-H simulation with that in which the urban region is removed (NOCITY-H) (Fig. 6), it is apparent that convection does not develop downwind of where the city would have been located. Convection does, however, develop to the southwest of where the city would have been, as it does in the RURAL-H simulation. This result holds true for all of the other simulations in which the urban region is removed, irrespective of the aerosol source functions used in the location of the city (not shown). It also holds true for the set of simulations with cleaner or rural background aerosol concentrations (not shown). This result demonstrates that urban land use has a greater impact than does the presence of urban-enhanced aerosol on whether convection actually develops downwind of an urban region. These findings

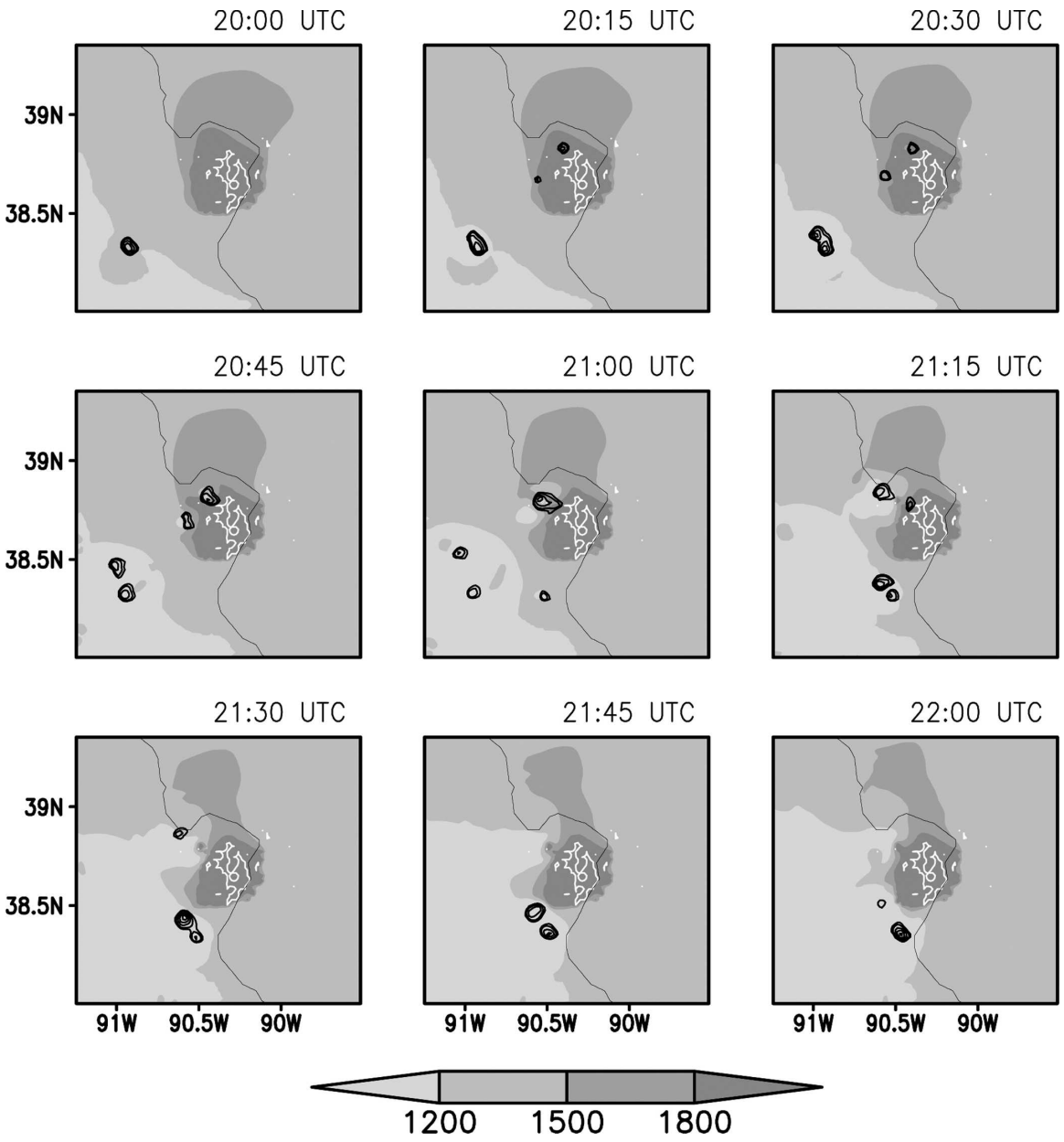

FIG. 7. Same as in Fig. 5, but for the URBAN-H sensitivity test.

are consistent with the hypothesis of Shepherd and Burian (2003) in which they speculate that the dynamic processes induced by urban regions are more dominant than aerosol impacts on urban-induced convective events, as well as with the observations of Jin et al. (2005) that urban rainfall anomalies are not fully related to changes in aerosol.

The storm development that occurs when including the effects of both urban-enhanced CCN and GCCN (URBAN-H) is shown in Fig. 7. It is apparent from this figure that the location of the updraft development is similar to that when only the rural aerosol concentrations are utilized (RURAL-H). However, the storm due north of the city develops about 15 min earlier in the URBAN-H simulation and is stronger than its rural counterpart. This difference highlights the impact that variations in aerosol concentrations can have on the dynamics of the storm. The stronger updrafts then influence the amount of precipitation produced at the surface, as will be seen below.

In Fig. 8 the total water mass for the different hydrometeors in the downwind region is represented as

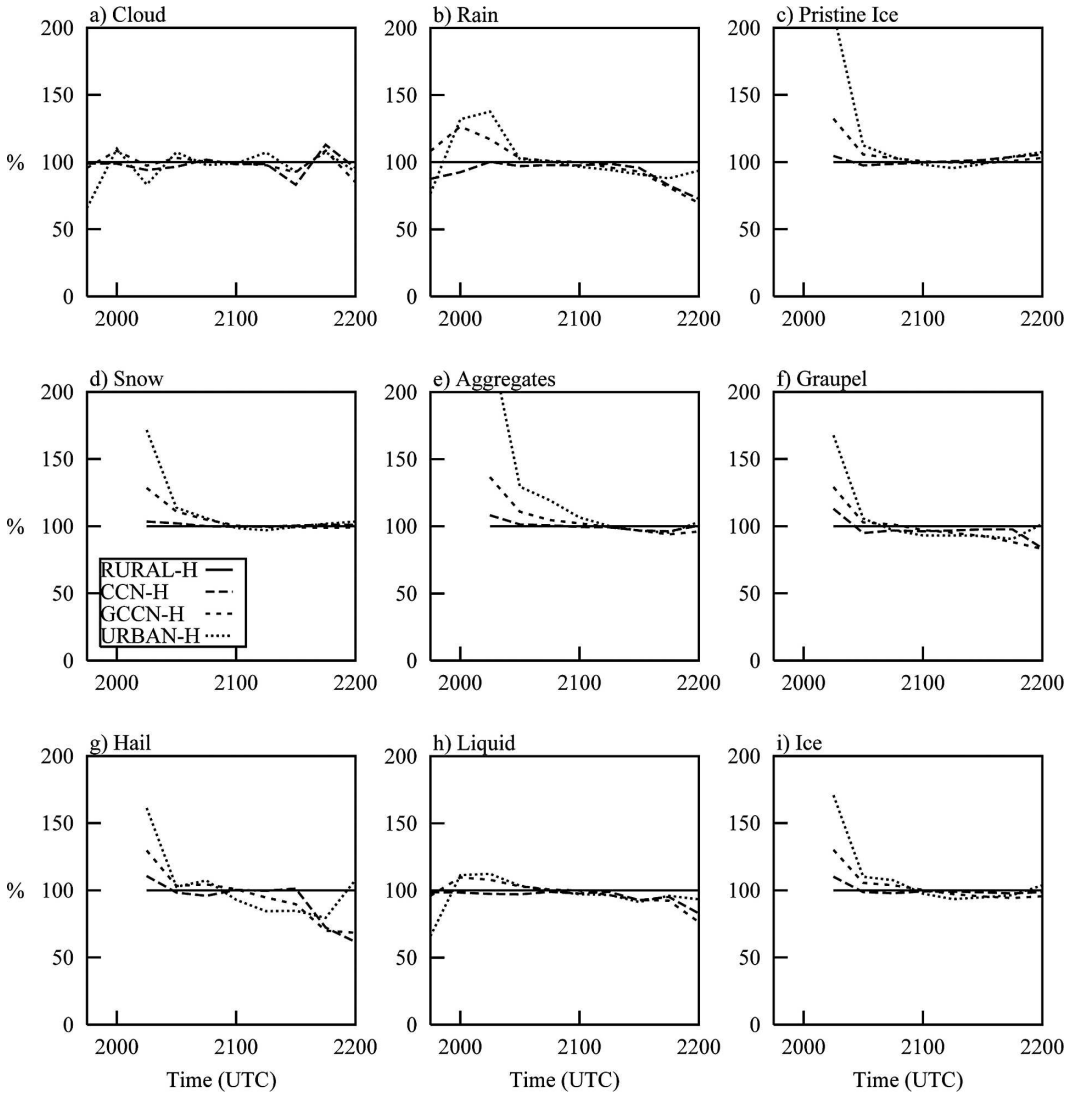

FIG. 8. Time series of the total hydrometeor mass (vertically and horizontally integrated) within the downwind region for the high-background-concentration sensitivity tests, expressed as a percentage of the RURAL-H output. (h) Liquid and (i) ice represent the total of the liquid and ice species, respectively.

a time series of the percentage of the corresponding RURAL-H hydrometeors. It is apparent from the figure that enhancements in GCCN (GCCN-H) and both GCCN and CCN (URBAN-H) result in a more rapid warm-rain process, generating 40%–50% more rain than in the RURAL-H case between 1945 and 2030 UTC, whereas enhanced CCN concentrations (CCN-H) suppress the warm-rain process during this time. After 2030 UTC the differences in rain between the simulations are small, and eventually rain production in the RURAL-H case dominates after 2145 UTC. Differences in cloud water amounts between the simulations are small, being on the order of 5%–10%, with specific trends not being obvious. Until about 2115 UTC, all of the ice species amounts are greatest in the URBAN-H case, followed by that in which only GCCN are enhanced. This result is associated with the stronger updrafts in these cases, as well as the greater amounts of rainwater being available for freezing and binary interactions with ice species already present. Differences between the CCN-H and the RURAL-H case are small during the same time period.

The accumulated volumetric precipitation, expressed as a percentage of the control (RURAL-H) simulation, is shown as a time series in Fig. 9. Until 2115 UTC, the simulations in which GCCN or both GCCN and CCN are enhanced produce more precipitation than does the control simulation, and enhanced concentrations of

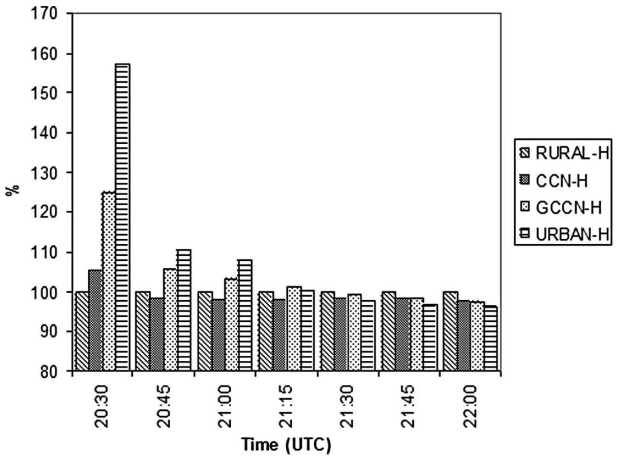

FIG. 9. Time series of the accumulated volumetric precipitation in the downwind region expressed as a percentage of the RURAL-H simulation.

CCN reduce the downwind precipitation. After 2030 UTC, the differences in magnitude are on the order of 5%–10%. However, as the simulation progresses, the greatest precipitation is produced in the situation in which the air is the cleanest.

This series of experiments, in which the background aerosol concentrations are high, demonstrates that urban-enhanced aerosols have an impact on both the dynamical and microphysical characteristics of the convection developing downwind of the urban region. The results from the sensitivity tests in which lower CCN and GCCN rural concentrations were employed while still making use of the same urban concentrations as those in the higher background concentration tests (see Table 2) will now be discussed.

5. Lower background aerosol concentration results

The storm developments in the RURAL-L and URBAN-L simulations are shown in Fig. 10 and Fig. 11, respectively. As with the high background case, the enhanced aerosol concentrations associated with the urban regions influence the timing and strength of the developing updrafts; however, the differences are more significant and there are further differences between these simulations. The storm to the north of the city splits at 2115 UTC in the RURAL-L simulation. Although this splitting does occur in the lower levels in the URBAN-L simulation, it is not evident in the upper levels. Note also that a new storm begins to develop to the northwest of the city around 2200 UTC in the RURAL-L run, but this development is not observed in the URBAN-L simulation. The storm-splitting process is affected by the strength of the cold pools produced by these storms, which is influenced by the amount of precipitation produced and the size of the raindrops and hail. These in turn are affected by the urban aerosol concentrations. The reasons for the differences in the storm development and dynamics when urban-enhanced aerosols are present are analyzed in detail in a paper currently in preparation.

Urban-enhanced aerosol concentrations therefore appear to exert a significant influence on the storm dynamics of the convection developing downwind of the urban region. This is also apparent in Fig. 12 in which time series of the maximum updraft strengths and the average of the maximum updrafts at each point for the downwind region are shown. Both of these fields demonstrate that stronger updrafts are produced between 2000 and approximately 2100 UTC in the simulations in which GCCN or both GCCN and CCN are enhanced. After 2100 UTC, the updrafts in the CCN-L and RURAL-L simulations are then greater, as is clearly obvious in the averaged output (Fig. 12b), with the simulation in which CCN are enhanced being predominant. The change in these trends coincides with the time of the storm splitting. The development of new updrafts downwind of the city in the RURAL-L and CCN-L cases is also obvious around 2145 UTC. The downdrafts (Fig. 13) follow a trend that is similar to those of the updrafts, being greater initially in the simulations in which GCCN are enhanced (GCCN-L and URBAN-L), and only developing later in the RURAL-L and CCN-L runs.

Times series of the total hydrometeor masses downwind of the city (Fig. 14) demonstrate that cloud water forms more rapidly between 2000 and 2045 UTC in the simulations in which the GCCN are enhanced (GCCN-L and URBAN-L), whereas enhanced CCN concentrations result in a slower cloud water production during the same time period. After this time, however, the trend reverses, with the RURAL-L and CCN-L producing more cloud water. The differences in cloud water amounts are on the order of 30%. The enhanced warm-rain process is evident in the simulations in which GCCN are higher (GCCN-L and URBAN-L) between 2000 and 2100 UTC. After this time, the trend reverses, as with the cloud water, and more rain is formed in the RURAL-L and CCN-L cases. Similar trends are evident for all of the ice species, too, and are indicative of the greater amounts of liquid water available for freezing and interactions between the ice and liquid water species, as well as the stronger updrafts that transport water to higher levels in the cloud. The time period in which the reversal of these trends becomes obvious coincides with the time period in which the storm splitting occurs, which once

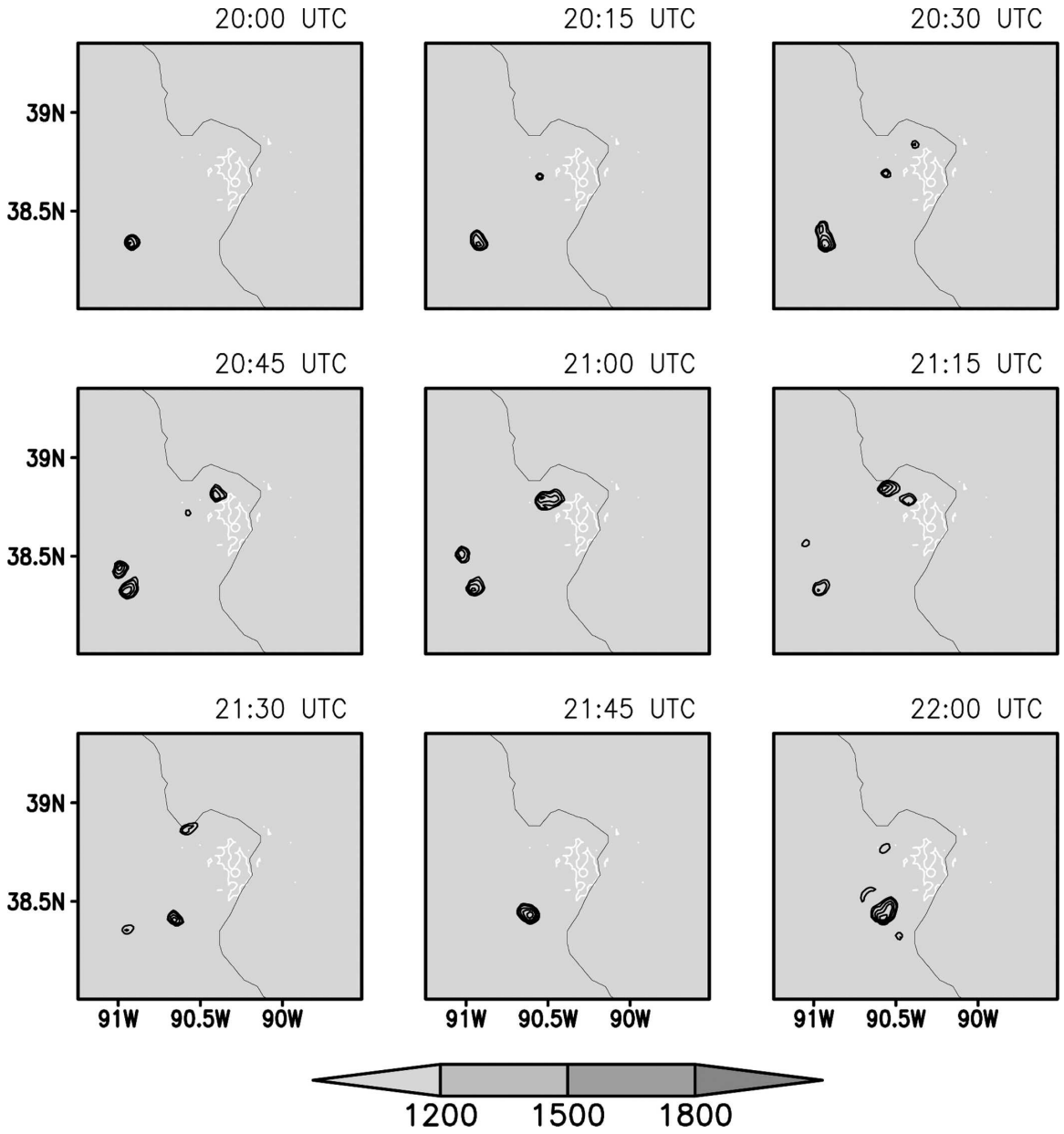

FIG. 10. Same as in Fig. 5, but for the RURAL-L simulation.

again emphasizes the inseparable link between the microphysics and the dynamics. It also illustrates how nonlinear the response of clouds to varying amounts of aerosol concentrations becomes once precipitation is altered.

The vertical distribution of cloud water and rain within the updraft (averaged over the region within a 15-km radius of the maximum updraft) for various times is shown in Fig. 15. A similar plot for the ice species is shown in Fig. 16. The rapid formation of cloud water and rain associated with the presence of enhanced GCCN (GCCN-L and URBAN-L) is evident at 2000 UTC (Figs. 15a,b), as is the delayed response in the formation of these species in the presence of urban-enhanced CCN (CCN-L). Rain reaches the surface first in the GCCN-L and URBAN-L cases and coincides with the time period of the strongest initial downdrafts (Fig. 13). The surface rainfall in these cases then becomes less than in the control case (RURAL-L), whereas the CCN-L produces slightly more rain. These simulations emphasize the enhancement of the warm-rain process in those simulations in which GCCN are

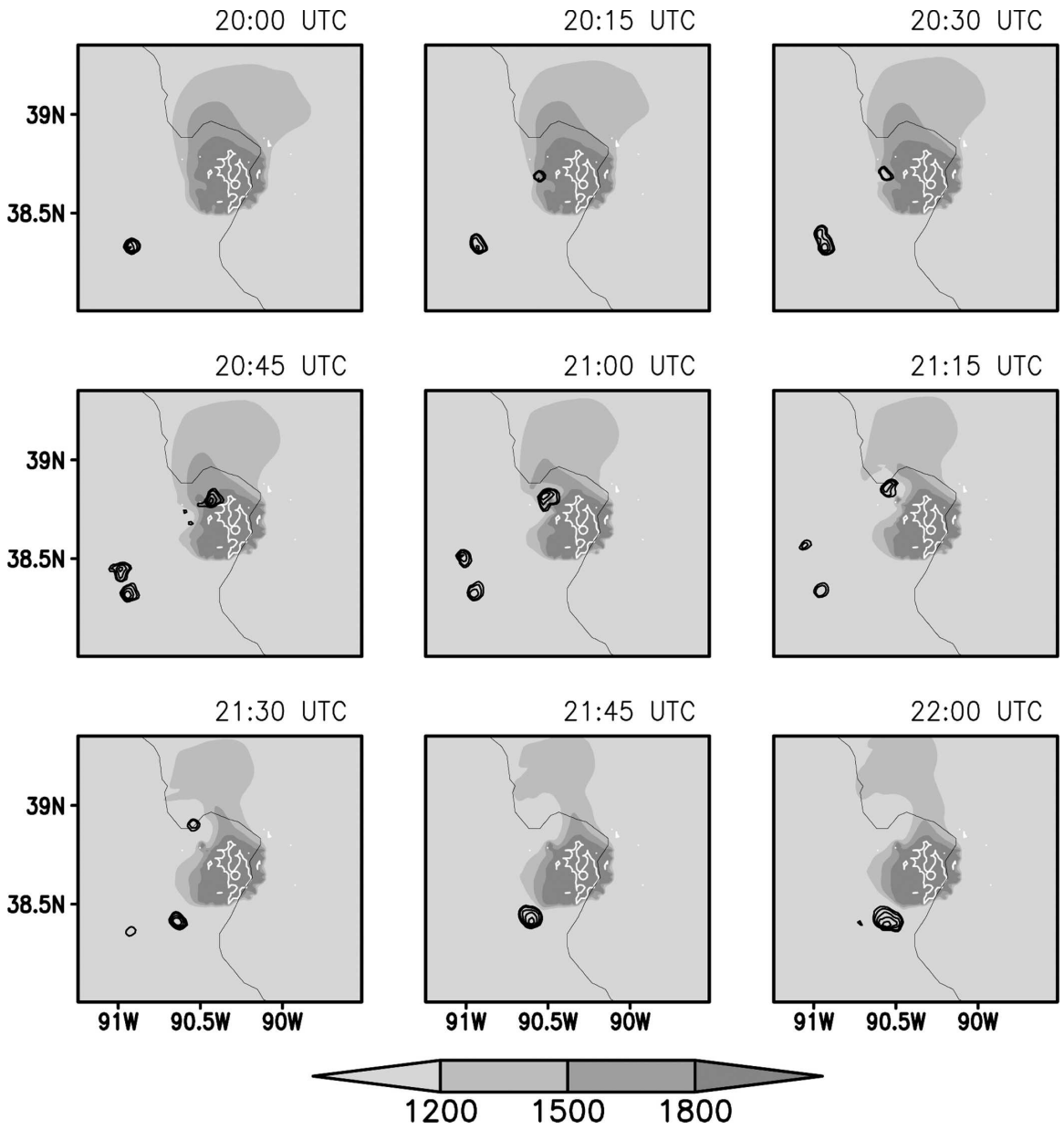

FIG. 11. Same as in Fig. 5, but for the URBAN-L simulation.

enhanced and the suppression of cloud water and rain formation in the cases in which CCN alone are enhanced.

The stronger updrafts and greater amounts of supercooled liquid water at 2000 UTC in the GCCN-L and URBAN-L cases result in enhanced mixing ratios of all of the ice species by 2030 UTC, whereas the delayed cloud water and rain formation in the CCN-L case is associated with the delay in the formation of all of the ice species in this case (Fig. 16). Such enhancements in the graupel and hail mixing ratios in the GCCN-L and URBAN-L cases due to the greater availability of supercooled water are likely to be associated with corresponding increases in lightning frequency over and downwind of the urban region, as was discussed by Takahashi (1978). Flash densities for St. Louis and the surrounding region were determined for 8 June 1999 using National Lightning Detection Network (NLDN) data and are shown in Fig. 17. It is apparent from this figure that higher flash densities were observed over and downwind of St. Louis when compared with the surrounding regions. As time progresses and more cloud and rainwater are produced in the CCN-L run, a corresponding increase in the graupel and hail mixing

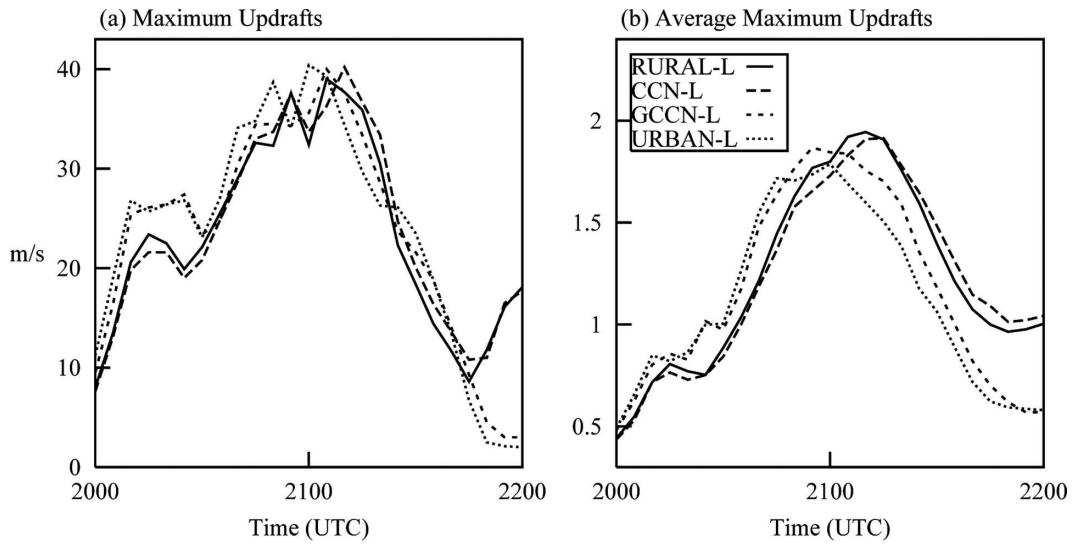

FIG. 12. Time series of (a) the maximum updraft within the downwind region and (b) the average of the maximum updraft at each point in the downwind region for the sensitivity tests described in the text.

ratios, when compared with the control (RURAL-L) simulation, becomes apparent. However, the differences in magnitude tend to be less than those in the GCCN-L and URBAN-L cases as a result of less cloud and rainwater being produced in the CCN-L simulation.

Enhancing GCCN and both GCCN and CCN produces greater amounts of accumulated precipitation downwind of the city from the time that convection begins to about 2130 UTC (Fig. 18). After 2130 UTC, following the changes in the storm dynamics and the development of the new storm to the northwest of the urban region, greater amounts of precipitation are produced downwind of the city in the RURAL-L case. Enhanced CCN concentrations suppress the production of precipitation downwind of the city throughout the simulation, although less so after 2130 UTC. These trends are similar to those for the higher-background-concentration cases; however, the differences between the simulations in this series of tests are as high as 30% (after 2030 UTC), which is significantly greater than in the higher-background-aerosol cases. The difference in the accumulated surface precipitation between the RURAL-L and URBAN-L simulations is shown in Fig. 19 at half-hourly intervals. Note that the difference is taken using the precipitation accumulated from the beginning of the simulation up to the time indicated on each panel in the figure and not just for the precipitation accumulated in each half-hour period. Figure 19 demonstrates the more rapid production of precipitation over a larger area in the URBAN-L simulation initially, as well as the greater amounts of precipitation produced in the RURAL-L case after 2130 UTC, which are associated with the changes in storm dynamics and the development of the new storm to the northwest of the city. It is also apparent from Fig. 19 that not only are the amounts of surface precipitation affected by variations in aerosol concentrations, but the spatial distribution with respect to the city is also influenced.

6. Conclusions

Results of numerical experiments designed to investigate the impacts of urban-enhanced aerosol on the development of convection and precipitation over and

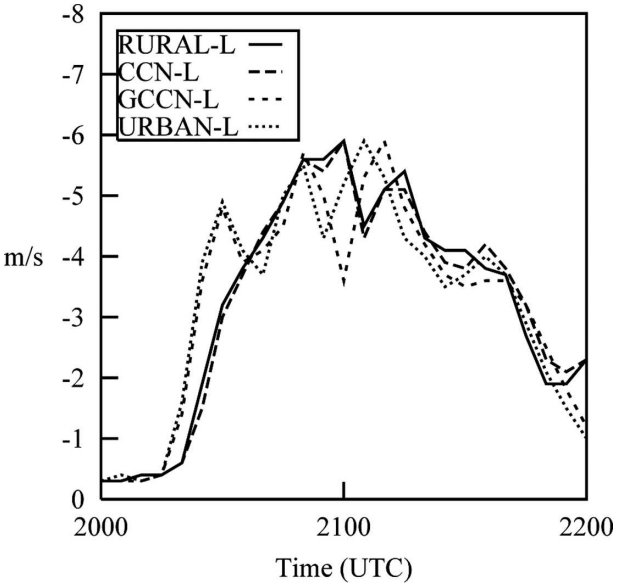

FIG. 13. Time series of the maximum downdraft within the downwind region for the sensitivity tests described in the text.

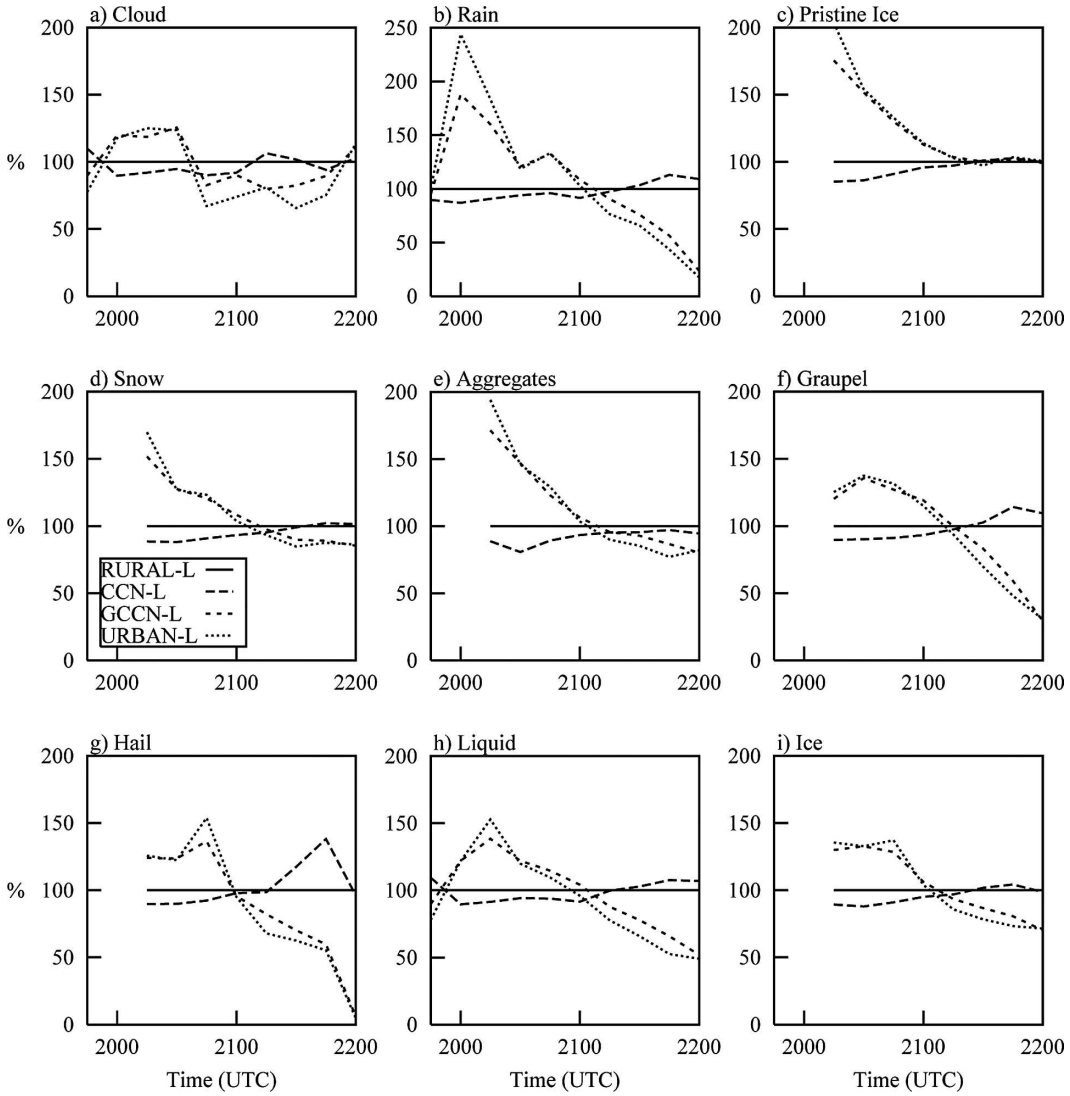

FIG. 14. Same as in Fig. 8, but for the lower background aerosol concentration tests.

downwind of urban regions have been presented. The experiments were performed using a cloud-resolving model that incorporates both sophisticated surface processes and aerosol processes, thus allowing for a comparison of the relative importance of these influences. It is apparent from the model output that, while urban-enhanced aerosols have numerous effects on the microphysics and dynamics of the downwind convective storms, it is the convergence effects driven by the urban land use characteristics that determine whether convection will actually develop. Storms did not develop in the vicinity of the city in the simulations in which the urban region was excluded, even if the urban-enhanced aerosol concentrations were maintained in the region where the city would have been located. However, once storms did develop downwind of the urban region, the presence of urban-enhanced CCN and GCCN exerts a significant effect on numerous microphysical, dynamical, and precipitation characteristics of these storms.

It was found that, when GCCN or both CCN and GCCN concentrations were enhanced, cloud water and rain formed more rapidly than in the control simulation in which only rural aerosol concentrations were utilized. The updrafts were also stronger initially, and the downdrafts developed more quickly. The larger amounts of supercooled liquid water available, together with the stronger updrafts, led to the generation of greater ice mixing ratios earlier in the storm development. This could be expected to be associated with more frequent lightning strikes at this stage. Greater amounts of surface precipitation were also produced in these cases during the first 1.25–1.5 h. When CCN alone

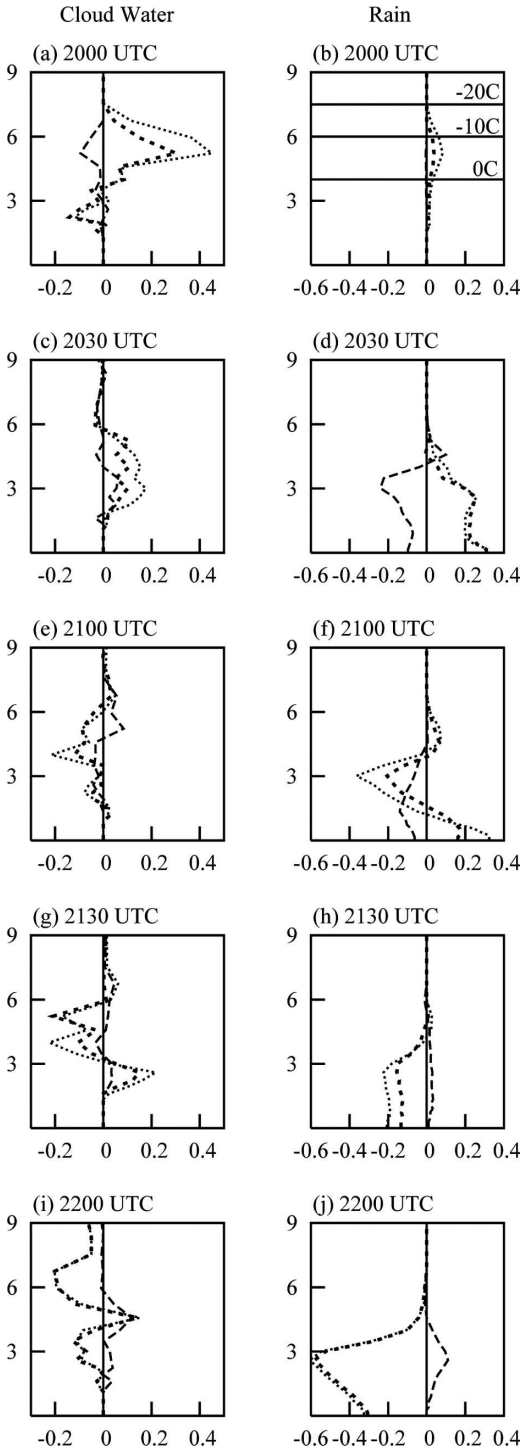

FIG. 15. Time series of the (left) cloud and (right) rain mixing ratios averaged across the updraft regions for the experiments described in the text. The experiments may be identified using the key in Fig. 14. The horizontal lines in (b) are isotherms. The abscissa is mixing ratio (g kg^{-1}), and the ordinate is height (km).

were enhanced, the formation of cloud water, rain, and all of the ice species was delayed, as was the development of both the updrafts and downdrafts. The total mass of the liquid and ice species produced was also less, and the surface precipitation was suppressed in the presence of urban-enhanced CCN concentrations.

Strong microphysical–dynamical interactions are evident in these results. The rapid formation of the liquid water and ice species in the cases in which GCCN and both GCCN and CCN are enhanced leads to a strengthening of the updraft, which in turn deepens the storm system and produces more liquid water and ice. However, the greater and more rapid production of surface precipitation generates stronger downdrafts and more intense cold pools earlier in the storm life cycle than in the control simulation. This is detrimental to the updraft development and strength, the evidence of which is the earlier demise of the storm closest to the urban region following storm splitting and the absence of new convective storm development downwind of the urban region at about 2200 UTC that was observed to occur in the control simulation. In the CCN-enhanced simulation, although the updrafts develop later in association with the delayed hydrometeor development, they are eventually stronger than those in the simulations in which GCCN or both GCCN and CCN are enhanced. Like those in the control run, the storms last longer following storm splitting, and new storm development occurs downwind of the city later on in the simulation. This results in greater amounts of liquid water and ice being produced between 2100 and 2200 UTC than in the GCCN and URBAN simulations, as well as increased amounts of accumulated surface precipitation during this time. The variations in storm dynamics in response to variations in the microphysics result in the greatest accumulated surface precipitation in the GCCN and URBAN cases between 2030 and 2130 UTC. However, as the simulation progresses, this trend reverses, and by 2200 UTC more surface precipitation has accumulated in the control case, closely followed by the CCN-L run. It appears that the delay in the updraft and downdraft development in the CCN-L case and the influence of this on the storm dynamics and subsequent storm development tend to offset, to some degree, the adverse effects of the suppressed warm-rain process. This finding appears to be consistent with the observations of Khain et al. (2005) that, under certain atmospheric conditions, greater CCN concentrations can enhance rather than reduce surface precipitation, through the dynamic effect of aerosols, which was found to produce stronger secondary clouds, the subsequent formation of a squall line, and heavy precipitation. The *extremely complex, nonlinear relationships* between the

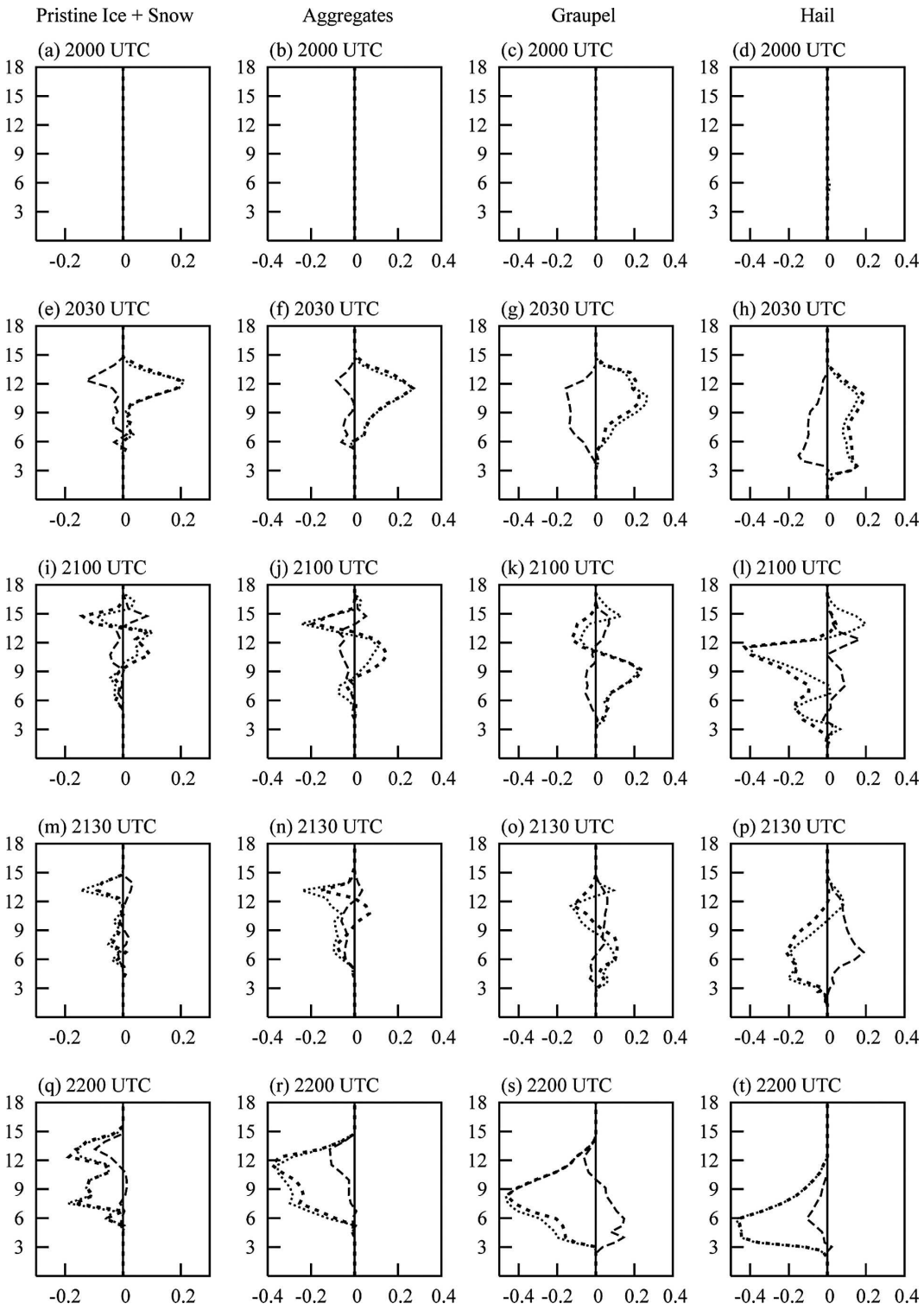

FIG. 16. Same as in Fig. 15, but for the ice species.

microphysics and dynamics therefore *make it difficult to make absolute statements regarding the impacts* of urban-enhanced CCN and GCCN on downwind convection and precipitation.

Although the trends associated with variations in urban-enhanced CCN and GCCN concentrations were similar in the lower and higher background aerosol concentration cases, the magnitude of the aerosol influ-

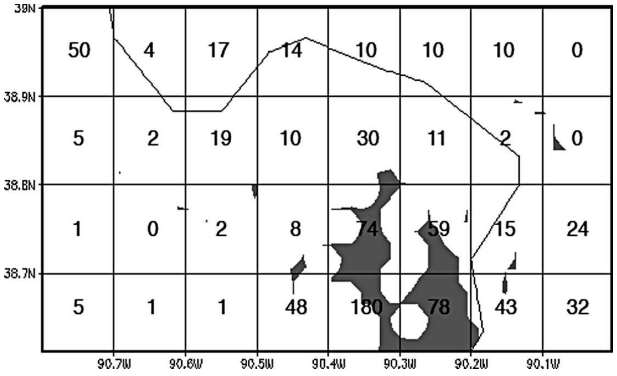

FIG. 17. Lightning flash density (flashes per kilometer per day, multiplied by 100) calculated using NLDN data for 8 Jun 1999 in the region of St. Louis. Shading indicates the location of St. Louis.

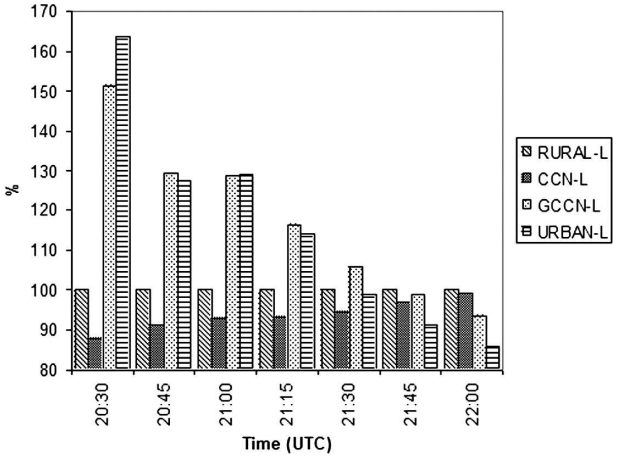

FIG. 18. Same as in Fig. 9, but for the lower-background-aerosol-concentration tests.

ences decreases with increasing background/rural aerosol concentrations. This result suggests that urban aerosol effects on downwind convection and precipitation could be expected to be greater in less industrialized regions of the United States, as well as in countries such as Canada and Australia, where the background aerosol concentrations are generally lower. Likewise, in coastal areas where sea-breeze circulations may transport clean background aerosol over urban centers, the response to urban pollution could be very large.

Last, note that these aerosol experiments have only been performed for a *specific* case study with a *particular* set of atmospheric conditions. As such, great caution

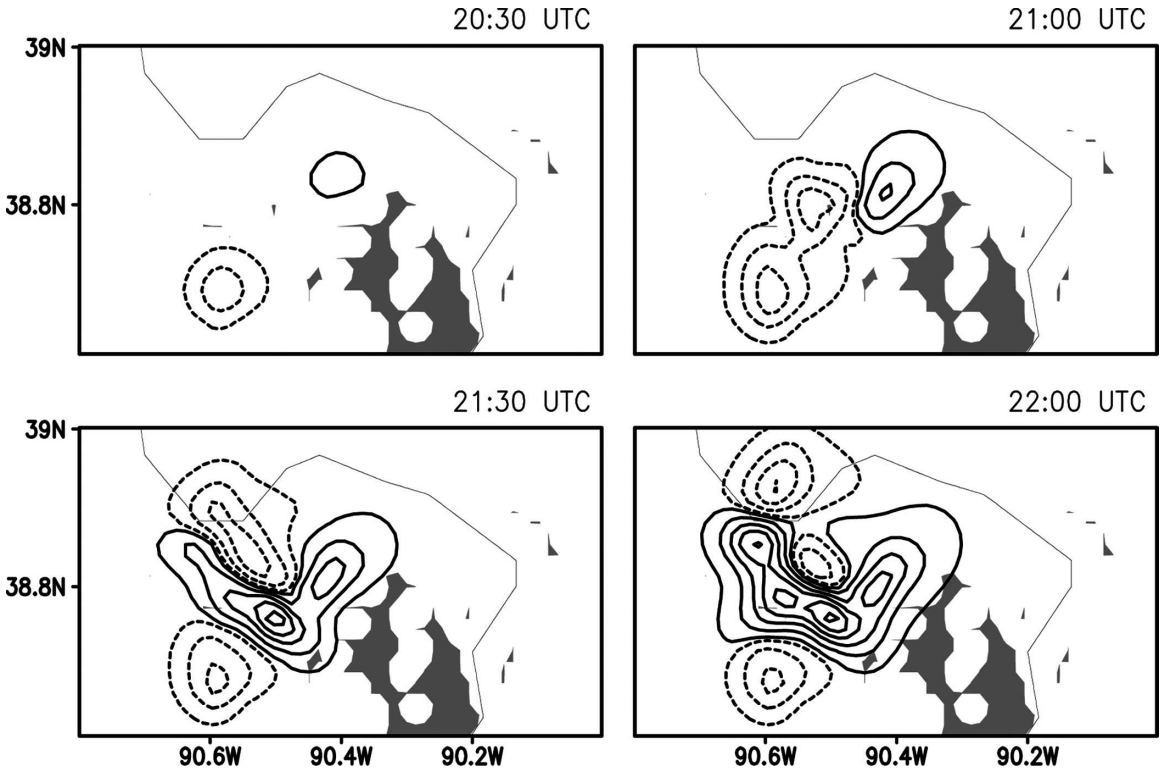

FIG. 19. RURAL-L − URBAN-L accumulated surface precipitation at half-hourly intervals. Solid lines indicate positive values, and dashed lines represent negative values. The contour interval is 5 mm. The 1-mm isoline is shown, and the 0-mm isoline is excluded. The shading represents the location of the urban region.

must be exercised when drawing generalized conclusions about the impacts of urban-enhanced aerosol on downwind convective storms. In future research, further sensitivity tests need to be conducted for a wide range of environmental conditions, urban regions, and aerosol concentrations.

Acknowledgments. This research was funded by the National Science Foundation under Grant ATM-0327652 and by the National Oceanic and Atmospheric Administration under Grant NAS5-99237. We gratefully acknowledge Dr. Valery Masson (Centre National de Recherches Météorologiques) for the use of the Town Energy Budget model. Chris Rozoff is thanked for the use of his code. The comments of three anonymous reviewers have resulted in an improved manuscript.

REFERENCES

Andreae, M. O., D. Rosenfeld, P. Artaxo, A. A. Costa, G. P. Frank, K. M. Longo, and M. A. F. Silva-Dias, 2004: Smoking rain clouds over the Amazon. *Science,* **303,** 1337–1342.

Auer, A. H., Jr., 1975: The production of cloud and Aitken nuclei by the St. Louis metropolitan area (Project METROMEX). *J. Rech. Atmos.,* **9,** 11–22.

Baik, J.-J., and Y.-H. Kim, 2001: Dry and moist convection forced by an urban heat island. *J. Appl. Meteor.,* **40,** 1462–1475.

Balling, R. C., and S. W. Brazel, 1987: Recent changes in Phoenix, Arizona, summertime diurnal precipitation patterns. *Theor. Appl. Climatol.,* **38,** 50–54.

Bornstein, R., and Q. Lin, 2000: Urban heat islands and summertime convective thunderstorms in Atlanta: Three case studies. *Atmos. Environ.,* **34,** 507–516.

Borys, R. D., D. H. Lowenthal, and D. L. Mitchell, 2000: The relationship among cloud microphysics, chemistry and precipitation rate in cold mountain clouds. *Atmos. Environ.,* **34,** 2593–2602.

——, ——, S. A. Cohn, and W. O. J. Brown, 2003: Mountaintop and radar measurements of anthropogenic aerosol effects on snow growth and snowfall rate. *Geophys. Res. Lett.,* **30,** 1538, doi:10.1029/2002GL016855.

Braham, R. R., 1974: Information content of CCN spectra vs. measurements at a single supersaturation. Preprints, *Conf. on Cloud Physics,* Tucson, AZ, Amer. Meteor. Soc., 9–12.

——, 1976: Modification of clouds and weather by a large metropolitan area. Preprints, *Second WMO Scientific Conf. on Weather Modification,* Boulder, CO, WMO, 435–442.

——, 1977: University of Chicago contribution to Project METROMEX-11. Cloud Physics Laboratory, Department of Geophysical Science, University of Chicago Tech. Note 50, Final Tech. Rep. to the National Science Foundation, 105 pp.

——, and P. Spyers-Duran, 1974: Nucleus measurements in an urban atmosphere. *J. Appl. Meteor.,* **13,** 940–945.

Braham, R. R., Jr., R. G. Semonin, A. H. Auer, S. A. Changnon Jr., and J. M. Hales, 1981: Summary of urban effects on clouds and rain. *METROMEX: A Review and Summary, Meteor. Monogr.,* No. 40, Amer. Meteor. Soc., 141–152.

Changnon, S. A., 1979: Rainfall changes in summer caused by St. Louis. *Science,* **205,** 402–404.

——, R. G. Semonin, A. H. Auer, R. R. Braham, and J. M. Hales, 1981: *METROMEX: A Review and Summary. Meteor. Monogr.,* No. 40, Amer. Meteor. Soc., 181 pp.

——, R. T. Shealy, and R. W. Scott, 1991: Precipitation changes in fall, winter, and spring caused by St. Louis. *J. Appl. Meteor.,* **30,** 126–134.

Cooper, W. A., R. T. Bruintjes, and G. K. Mather, 1997: Calculations pertaining to hygroscopic seeding with flares. *J. Appl. Meteor.,* **36,** 1449–1469.

Cotton, W. R., 1972a: Numerical simulation of precipitation development in supercooled cumuli—Part I. *Mon. Wea. Rev.,* **100,** 757–763.

——, 1972b: Numerical simulation of precipitation development in supercooled cumuli—Part II. *Mon. Wea. Rev.,* **100,** 764–784.

——, and R. A. Pielke, 1995: *Human Impacts on Weather and Climate*. Cambridge University Press, 288 pp.

——, and Coauthors, 2003: RAMS 2001: Current status and future directions. *Meteor. Atmos. Phys.,* **82,** 5–29.

Craig, K., and R. Bornstein, 2002: MM5 simulation of urban induced convective precipitation over Atlanta. Preprints, *Fourth Symp. on the Urban Environment,* Norfolk, VA, Amer. Meteor. Soc., 5–6.

Dickinson, R. E., A. Henderson-Sellers, P. J. Kennedy, and M. F. Wilson, 1986: Biosphere–Atmosphere Transfer Scheme (BATS) for the NCAR Community Climate Model. NCAR Tech. Rep. NCAR/TN275+STR, 69 pp.

Diem, J. E., and D. P. Brown, 2003: Anthropogenic impacts on summer precipitation in central Arizona, U.S.A. *Prof. Geogr.,* **55,** 343–355.

Dixon, P. G., and T. L. Mote, 2003: Patterns and causes of Atlanta's urban heat island–initiated precipitation. *J. Appl. Meteor.,* **42,** 1273–1284.

Feingold, G., and A. J. Heymsfield, 1992: Parameterizations of condensational growth of droplets for use in general circulation models. *J. Atmos. Sci.,* **49,** 2325–2342.

——, S. Tzivion, and Z. Levin, 1988: Evolution of raindrop spectra. Part I: Solution to the stochastic collection/breakup equation using the method of moments. *J. Atmos. Sci.,* **45,** 3387–3399.

——, R. L. Walko, B. Stevens, and W. R. Cotton, 1998: Simulations of marine stratocumulus using a new microphysical parameterization scheme. *Atmos. Res.,* **47–48,** 505–528.

——, W. R. Cotton, S. M. Kreidenweis, and J. T. Davis, 1999: The impact of giant cloud condensation nuclei on drizzle formation in stratocumulus: Implications for cloud radiative properties. *J. Atmos. Sci.,* **56,** 4100–4117.

Givati, A., and D. Rosenfeld, 2004: Quantifying precipitation suppression due to air pollution. *J. Appl. Meteor.,* **43,** 1038–1056.

Gunn, R., and B. B. Phillips, 1957: An experimental investigation of the effect of air pollution on the initiation of rain. *J. Meteor.,* **14,** 272–280.

Harrington, J. Y., 1997: The effects of radiative and microphysical processes on simulated warm and transition season Arctic stratus. Ph.D. dissertation, Colorado State University, 289 pp. [Available from Department of Atmospheric Science, Colorado State University, Fort Collins, CO 80523.]

Hill, G. E., 1974: Factors controlling the size and spacing of cumulus clouds as revealed by numerical experiments. *J. Atmos. Sci.,* **31,** 646–673.

Hindman, E. E., II, P. V. Hobbs, and L. F. Radke, 1977a: Cloud condensation nuclei from a paper mill. Part I: Measured effects on clouds. *J. Appl. Meteor.,* **16,** 745–752.

——, P. M. Tag, B. A. Silverman, and P. V. Hobbs, 1977b: Cloud condensation nuclei from a paper mill. Part II: Calculated effects on rainfall. *J. Appl. Meteor.,* **16,** 753–755.

Hjelmfelt, M. R., 1982: Numerical simulation of the effects of St. Louis on mesoscale boundary-layer airflow and vertical motion: Simulations of urban vs non-urban effects. *J. Appl. Meteor.,* **21,** 1239–1257.

Huff, F. A., and J. L. Vogel, 1978: Urban, topographic and diurnal effects on rainfall in the St. Louis region. *J. Appl. Meteor.,* **17,** 565–577.

Jaurequi, E., and E. Romales, 1996: Urban effects on convective precipitation in Mexico City. *Atmos. Environ.,* **30,** 3383–3389.

Jin, M., J. M. Shepherd, and M. D. King, 2005: Urban aerosols and their variations with clouds and rainfall: A case study for New York and Houston. *J. Geophys. Res.,* **110,** D10S20, doi:10.1029/2004JD005081.

Jirak, I. L., and W. R. Cotton, 2006: Effect of air pollution on precipitation along the Front Range of the Rocky Mountains. *J. Appl. Meteor. Climatol.,* **45,** 236–245.

Johnson, D. B., 1976: Ultragiant urban aerosol particles. *Science,* **194,** 941–942.

Kessler, E., 1969: *On the Distribution and Continuity of Water Substance in Atmospheric Circulation. Meteor. Monogr.,* No. 32, Amer. Meteor. Soc., 84 pp.

Khain, A., D. Rosenfeld, and A. Pokrovsky, 2005: Aerosol impact on the dynamics and microphysics of deep convective clouds. *Quart. J. Roy. Meteor. Soc.,* **131,** 2639–2663.

Klemp, J. B., and R. B. Wilhelmson, 1978: The simulation of three-dimensional convective storm dynamics. *J. Atmos. Sci.,* **35,** 1070–1096.

Koenig, L. R., and F. W. Murray, 1976: Ice-bearing cumulus cloud evolution: Numerical simulations and general comparison against observations. *J. Appl. Meteor.,* **15,** 747–762.

Komp, M. J., and A. H. Auer Jr., 1978: Visibility reduction and accompanying aerosol evolution downwind of St. Louis. *J. Appl. Meteor.,* **17,** 1357–1367.

Lee, T. J., 1992: The impact of vegetation on the atmospheric boundary layer and convective storms. Ph.D. dissertation, Colorado State University, 137 pp.

Lilly, D. K., 1962: On the numerical simulation of buoyant convection. *Tellus,* **14,** 148–172.

Loose, T., and R. D. Bornstein, 1977: Observations of mesoscale effects on frontal movement through an urban area. *Mon. Wea. Rev.,* **105,** 563–571.

Lynn, B. H., A. P. Khain, J. Dudhia, D. Rosenfeld, A. Pokrovsky, and A. Seifert, 2005a: Spectral (bin) microphysics coupled with a mesoscale model (MM5). Part I: Model description and first results. *Mon. Wea. Rev.,* **133,** 44–58.

——, ——, ——, ——, ——, and ——, 2005b: Spectral (bin) microphysics coupled with a mesoscale model (MM5). Part II: Simulation of a CaPE rain even with a squall line. *Mon. Wea. Rev.,* **133,** 59–71.

Masson, V., 2000: A physically-based scheme for the urban energy budget in atmospheric models. *Bound.-Layer Meteor.,* **94,** 357–397.

——, C. S. B. Grimmond, and T. R. Oke, 2002: Evaluation of the Town Energy Budget (TEB) scheme with direct measurements from dry districts in two cities. *J. Appl. Meteor.,* **41,** 1011–1026.

Mather, G. K., 1991: Coalescence enhancement in large multicell storms caused by the emissions from a Kraft paper mill. *J. Appl. Meteor.,* **30,** 1134–1146.

Mesinger, F., and A. Arakawa, 1976: Numerical methods used in atmospheric models. GARP Publication Series, No. 14, WMO/ICSU Joint Organizing Committee, 64 pp.

Meyers, M. P., R. L. Walko, J. Y. Harrington, and W. R. Cotton, 1997: New RAMS cloud microphysics parameterization. Part II: The two-moment scheme. *Atmos. Res.,* **45,** 3–39.

Molders, N., and M. A. Olson, 2004: Impact of urban effects on precipitation in high latitudes. *J. Hydrometeor.,* **5,** 409–429.

Oke, T. R., 1988: The urban energy balance. *Prog. Phys. Geogr.,* **12,** 471–508.

Orville, R. E., and Coauthors, 2001: Enhancement of cloud-to-ground lightning over Houston, Texas. *Geophys. Res. Lett.,* **28,** 2597–2600.

Pielke, R. A., and Coauthors, 1992: A comprehensive meteorological modeling system—RAMS. *Meteor. Atmos. Phys.,* **49,** 69–91.

Ramanathan, V., P. J. Crutzen, J. T. Kiehl, and D. Rosenfeld, 2001: Aerosols, climate, and the hydrological cycle. *Science,* **294,** 2119–2124.

Reisin, T., Z. Levin, and S. Tzivion, 1996: Rain production in convective clouds as simulated in as axisymmetric model with detailed microphysics. Part II: Effects of varying drops and ice initiation. *J. Atmos. Sci.,* **53,** 1815–1837.

Rogers, E., T. L. Black, D. G. Deaven, G. J. DiMego, Q. Zhao, M. E. Baldwin, N. W. Junker, and Y. Lin, 1996: Changes to the operational "early" Eta analysis/forecast system at the National Centers for Environmental Prediction. *Wea. Forecasting,* **11,** 391–416.

Rosenfeld, D., 1999: TRMM observed first direct evidence of smoke from forest fires inhibiting rainfall. *Geophys. Res. Lett.,* **26,** 3105–3108.

——, 2000: Suppression of rain and snow by urban air pollution. *Science,* **287,** 1793–1796.

Rozoff, C. M., W. R. Cotton, and J. O. Adegoke, 2003: Simulation of St. Louis, Missouri, land use impacts on thunderstorms. *J. Appl. Meteor.,* **42,** 716–738.

Saleeby, S. M., and W. R. Cotton, 2004: A large-droplet mode and prognostic number concentration of cloud droplets in the Colorado State University Regional Atmospheric Modeling System (RAMS). Part I: Module descriptions and supercell test simulations. *J. Appl. Meteor.,* **43,** 182–195.

Scott, B. C., and P. V. Hobbs, 1977: A theoretical study of the evolution of mixed-phase cumulus clouds. *J. Atmos. Sci.,* **34,** 812–826.

Shepherd, J. M., 2005: A review of current investigations of urban-induced rainfall and recommendations for the future. *Earth Interactions,* **9**. [Available online at http://EarthInteractions.org.]

——, and S. J. Burian, 2003: Detection of urban-induced rainfall anomalies in a major coastal city. *Earth Interactions,* **7**. [Available online at http://EarthInteractions.org.]

——, H. Pierce, and A. J. Negri, 2002: Rainfall modification by major urban areas: Observations from spaceborne rain radar on the TRMM satellite. *J. Appl. Meteor.,* **41,** 689–701.

Smagorinsky, J., 1963: General circulation experiments with the primitive equations. Part I, The basic experiment. *Mon. Wea. Rev.,* **91,** 99–164.

Spyers-Duran, P., 1974: Cloud condensation nuclei measurements and estimates of production rates in the St. Louis urban complex. Preprints, *Fourth Conf. on Weather Modification,* Ft. Lauderdale, FL, Amer. Meteor. Soc., 390–395.

Squires, P., 1958: The microstructure and colloidal stability of warm clouds. *Tellus,* **10,** 256–271.

——, and T. Twomey, 1961: The relation between cloud drop

numbers and the spectrum of cloud nuclei. *Physics of Precipitation, Geophys. Monogr.,* No. 5, Amer. Geophys. Union, 211–219.

Stallins, J. A., M. L. Bentley, and L. S. Rose, 2006: Cloud-to-ground flash patterns for Atlanta, Georgia (USA) from 1992 to 2003. *Climate Res.,* **30,** 99–112.

Steiger, S. M., and R. E. Orville, 2003: Cloud-to-ground lightning enhancement over Southern Louisiana. *Geophys. Res. Lett.,* **30,** 1975, doi:10.1029/2003GL017923.

——, ——, and G. Hiffines, 2002: Cloud-to-ground lightning characteristics over Houston, Texas: 1989-2000. *J. Geophys. Res.,* **107,** 4117, doi:10.1029/2001JD001142.

Takahashi, T., 1978: Riming electrification as a charge generation mechanism in thunderstorms. *J. Atmos. Sci.,* **35,** 1536–1548.

Thielen, J., W. Wobrock, A. Gadian, P. G. Mestayer, and J.-D. Creutin, 2000: The possible influence of urban surfaces on rainfall development: A sensitivity study in 2D in the mesogamma scale. *Atmos. Res.,* **54,** 15–39.

van den Heever, S. C., G. G. Carrio, W. R. Cotton, P. J. DeMott, and A. J. Prenni, 2006: Impacts of nucleating aerosol on Florida storms. Part I: Mesoscale simulations. *J. Atmos. Sci.,* **63,** 1752–1775.

Walko, R. L., and Coauthors, 2000: Coupled atmosphere–biophysics–hydrology models for environmental modeling. *J. Appl. Meteor.,* **39,** 931–944.

Warner, J., 1968: A reduction in rainfall associated with smoke from sugar-cane fires—An inadvertent weather modification? *J. Appl. Meteor.,* **7,** 247–251.

——, and S. Twomey, 1967: The production of cloud nuclei by cane fires and the effects on cloud droplet concentration. *J. Atmos. Sci.,* **24,** 704–706.

Westcott, N. E., 1995: Summertime cloud-to-ground lightning activity around major Midwestern urban areas. *J. Appl. Meteor.,* **34,** 1633–1642.

Yin, Y., Z. Levin, T. Reisin, and S. Tzivion, 2000: Seeding convective clouds with hygroscopic flares: Numerical simulations using a cloud model with detailed microphysics. *J. Appl. Meteor.,* **39,** 1460–1472.